Modelling Sex-Specific Crossover Patterning in Arabidopsis

Lloyd, Andrew; Jenczewski, Eric

Published in:
Genetics

DOI:
10.1534/genetics.118.301838

Publication date:
2019

Citation for published version (APA):
Lloyd, A., & Jenczewski, E. (2019). Modelling Sex-Specific Crossover Patterning in Arabidopsis. *Genetics*, *211*(3), 847-859. https://doi.org/10.1534/genetics.118.301838

Modelling sex-specific crossover patterning in Arabidopsis

Andrew Lloyd[*, †] and Eric Jenczewski[†]

[*] Institute of Biological, Environmental and Rural Sciences, Aberystwyth University, Aberystwyth, SY23 3EB, UK

[†] Institut Jean-Pierre Bourgin, INRA, AgroParisTech, CNRS, Université Paris-Saclay, 78000, Versailles, France.

Short Title: Modelling crossovers in Arabidopsis

Keywords: recombination, crossovers, interference, beam-film, sex-specific

Corresponding author: Andrew Lloyd

Address: Institute of Biological, Environmental and Rural Sciences, Plas Gogerddan, Aberystwyth University, Aberystwyth, SY23 3EB, UK

Phone: +44 (0) 1970823229

Email: anl50@aber.ac.uk

ABSTRACT

Interference is a major force governing the patterning of meiotic crossovers. A leading model describing how interference influences crossover-patterning is the beam film model, a mechanical model based on the accumulation and redistribution of crossover-promoting stress along the chromosome axis. We use the beam-film model in conjunction with a large Arabidopsis reciprocal back-cross data set to gain mechanistic insights into the differences between male and female meiosis and crossover patterning. Beam-film modelling suggests that the underlying mechanics of crossover patterning and interference are identical in the two sexes, with the large difference in recombination rates and distributions able to be entirely explained by the shorter chromosome axes in females. The modelling supports previous indications that fewer crossovers occur via the class II pathway in female meiosis and that this could be explained by reduced DNA double strand breaks in female meiosis, paralleling the observed reduction in synaptonemal complex length between the two sexes. We also demonstrate that changes in the strength of suppression of neighboring class I crossovers can have opposite effects on effective interference depending on the distance between two genetic intervals.

INTRODUCTION

Meiotic crossovers shuffle parental genetic information generating new combinations of alleles. In most species the presence of one crossover inhibits nearby crossover formation so that the distances between crossovers are greater and more uniform, than if placed at random. This phenomenon, crossover interference, was first noted in genetic studies over a century ago

(1, 2), however it is only in the last few years that insights into its mechanistic basis have begun to surface.

The inhibitory effect of interference is thought to spread a defined distance along the chromosome axis, a linear proteinaceous structure formed by each chromosome at the base of the chromatin loop array in early prophase (reviewed 3). By mid-prophase, homologous chromosome axes are joined by additional proteins comprising the transverse filament and central element to form the synaptonemal complex (SC). Although the interference signal likely propagates prior to polymerization of the SC (3), the distance across which interference spreads is usually specified in μm SC, as SC length is easier to measure cytologically and is proportional to the length of the axis prior to synapsis. In yeast, interference is, at least in part, mediated by Topoisomerase II (4) and wild type levels of interference require SUMOylation of TopoII and the axis component Red1/Asy3 as well as ubiquitin-mediated removal of SUMOylated proteins (4). These findings are consistent with suggested roles for the chromosome axis and local stress relief via DNA remodeling, in mediating interference.

Several approaches have been used to model crossover (CO) patterning, the most notable being the gamma model and the beam-film model. The gamma model is a statistical model based on the observation that the distances between two crossovers are relatively uniform, following a gamma distribution (5–7). Under this model "effective interference strength" is highest when distances between crossovers show the least variation. This results in a large value of the gamma shape parameter.

In contrast, the beam-film model is a mechanistic model whose various parameters have biological correlates (8, 9). In the beam-film model, each bivalent has a number of precursor

sites (DSBs) that are subject to mechanical stress. CO designation at precursor sites is promoted by stress and this stress is relieved locally following CO-designation. As stress promotes COs, stress relief propagating out from crossover sites inhibits the formation of additional COs nearby. In the beam-film model, interference strength is highest when stress relief propagates furthest from designated crossover sites.

In most species, there are multiple crossover pathways. The majority of crossovers occur via the interference sensitive class I pathway and are dependent on the ZMM group of proteins identified initially in yeast (Zip1, Zip2, Zip3, Zip4, Mer3, Msh4, and Msh5) (10–17). Crossovers occurring via this pathway are specifically marked by Zip3/Hei10 and MLH1 foci at late pachytene (12, 18, 19). A number of secondary "clean-up" pathways repair DSBs not metabolized by the class I pathway (20, 21). These clean-up pathways mostly repair DSBs as non-crossovers, but also contribute a smaller number of crossovers (i.e. class II crossovers). Class II crossovers are insensitive to interference (6, 22, 23) and usually make up 10-30% of the total crossover number (e.g. 18, 22–24). In their simplest forms, the gamma and beam-film models deal exclusively with class I crossovers and several studies have explored crossover patterning in yeast using the single-pathway beam-film model (4, 9, 25, 26).

While the biological processes underlying meiosis and the various recombination pathways are remarkably conserved across eukaryotes (27), differences in crossover patterning exist both between and within species (27, 28). In Arabidopsis (29), as in many species (e.g. 30–33), there are marked sex-specific differences in crossover patterning. Recombination rates are highest in the male Arabidopsis germline, with particularly high levels of recombination in distal regions (29). In contrast, distal regions have the lowest recombination rates in female (29). Female meiosis has also been reported to have higher levels of interference (29). While these

differences have been repeatedly observed (29, 34), there has so far been little insight into the biological factors contributing to them. Beam-film modelling offers an attractive means to provide such insight, through estimating and comparing sex-specific values for the various model parameters, each of which has a biological correlate.

Theoretically such analyses are possible from both genetic and cytological data. However, while cytological analyses are routine in the Arabidopsis male germline, they remain challenging for female meiosis. In addition, as the number of crossovers per chromosome is low for female Arabidopsis, well over a thousand cells would need to be analyzed to achieve the same number of inter-interval distances (the limiting factor for analyses) commonly reported for yeast chromosomes (4, 9). For this reason, we took advantage of a previously published large Arabidopsis reciprocal backcross recombination data set (~1500 individuals and ~380 markers for both male and female) (29). Being genetically derived this dataset comprised crossovers arising from both the class I and class II recombination pathways.

To identify likely biological determinants of sex-specific differences in Arabidopsis crossover patterning we determined and compared sex-specific parameter values for various beam-film model parameters. In addition, we comprehensively explored the behavior of the two-pathway beam-film model, providing novel insights into how the patterning of class I and class II crossovers interact to influence patterns of inheritance. Such insights have not been possible from previous beam-film analyses focusing on the single-pathway model.

MATERIALS AND METHODS

Experimental data: Experimental dataset used has been previously published (29) and was derived from large Arabidopsis reciprocal backcross populations. On average, 1,505 plants

were genotyped for 380 SNPs in the male population and 1,507 plants genotyped for 386 SNPs in the female population (380 in common). As the average distance between markers is small in this data set – 316 kb in male, 311 kb in female – the number of double crossovers (DCOs) in a single interval are expected to be negligible (the average distance between DSBs is ~480 kb). It was therefore assumed during analysis that all recombination events were identifiable. Genotyping and recombination datasets are provided (Datasets S1 and S2 respectively).

Beam film parameter optimization: Beam-film simulations were performed and best-fit parameters determined using MADpatterns (25) and custom perl scripts with an approach based on that described in (9). For each chromosome and each sex at least three rounds of analysis were undertaken. In each round of each analysis 30,000 bivalents were simulated for a range of parameter values. In the first round, to ensure the full parameter space was sampled, relatively broad value ranges of optimised parameters (*Smax*: 2 - 10 L: 0.4 – 1.7; *T2Prob*: 0.002 - 0.008; *cL*: 0.3 - 1.3 and *cR*: 0.3 - 1.3) were chosen based on values described in Zhang et al (2014) and comparison of ad hoc simulations with analysis of experimental datasets (35). Parameters *N, B, E, Bs/Be/Bd, A* and *M* were set at appropriate default values (see below). In the next two rounds, progressively smaller step-sizes between values were used to arrive at the final parameter values. Descriptions of each parameter are provided below.

For each round of analysis, the crossover distributions, coefficient of co-incidence (CoC) curves and event distributions (distribution of number of COs per gamete) simulated for each chromosome were determined using MADpatterns (25) and compared to those obtained for the relevant sex and chromosome from the experimental data set. For crossover distributions and CoC curves, each chromosome was split into 13 equal sized adjacent intervals for analysis. Importantly the experimental data are gamete data, while the MADpatterns program simulates (and outputs) bivalent data (i.e. all crossovers on a pair of homologous chromosomes).

Therefore, all simulated bivalent crossover frequencies were halved to convert to gamete crossover frequencies. Bivalent event distributions were also converted to gamete event distributions, assuming random assignment of each crossover to two of the four chromatids i.e. each crossover has a 50% chance of being inherited by a gamete arising from that meiosis. Parameter sets were ranked based on the difference between simulated and experimentally determined CoC distributions [$Score_{CoC} = \Sigma_{IID}\ abs(\log_2(CoC_{sim}/CoC_{exp}))$], CO distributions [$Score_{CO} = \Sigma_{Int}\ (CO_{sim} - CO_{exp})^2$] and event distributions [$Score_{ED} = \Sigma_{Enum}\ (ED_{sim} - ED_{exp})^2$]. Simulations were ranked for each score and final parameter values chosen were those with the lowest rank-sum. For graphical representation, CoC curves were smoothed using locally estimated scatterplot smoothing (LOESS, span 0.3-0.5).

Optimized Parameters: Beam-film model parameters *Smax,* $L_{BF,}$ *cL/R* and T2Prob were optimized (see above). Parameters *N, B, E, Bs/Be/Bd, A* and *M* were fixed based on known values of the biological correlates, parameters that tend to be stable between species (9), or suggested default values (36). A description of each of these parameters is given below, further explanations can be found in refs. (9, 25).

Beam-film Parameters

The beam-film program requires three kinds of parameters: 1) precursor array parameters, which determine the position and number of potential crossover sites (DSBs) along each bivalent, 2) crossover patterning parameters, that determine which precursor sites become designated crossover sites and 3) the maturation efficiency parameter which determines the likelihood of designated crossover sites maturing to become true crossovers.

Precursor Array Parameters:

N – Precursor sites per bivalent: Parameter N sets the number of potential recombination sites or "precursors" on a bivalent. The biological correlate is the number of meiotic DSBs for that bivalent. For the first round of simulations we assumed 250 DSBs per meiosis in both male and female. For any given chromosome *N* was set to 250 × proportion total genome size (in Mb) contributed by that chromosome. For modelling of reduced DSB formation in female *N* we calculated as above assuming 150 DSBs genome wide.

B – Similarity in total precursor number between bivalents: B sets the similarity of precursor number between the multiple bivalents simulated for a given chromosome in each round of analysis. Precursor number for any given chromosome was set to be constant for each bivalent simulated ($B = 1$).

E – Evenness of precursor spacing: There is considerable experimental evidence that DSB spacing is non-random, being more evenly spaced than if placed at random (37, 38). For numerous organisms a parameter value of 0.6 has been found appropriate (9) and we therefore set *E* to 0.6 for all simulations (0 = random, 1 = even).

A – Intrinsic precursor sensitivities: In the early steps of the model each precursor is assigned a "sensitivity", reflecting the fact that not all DSBs have an equal chance of becoming a crossover; local factors e.g. SNP density, local structural diversity, epigenetic landscape may also influence the fate of each precursor site. Parameter *A* determines how precursor sensitivities are assigned. For all simulations *A* was set to 1 – sensitivities assigned from a uniform distribution.

Bs/Be/Bd – Recombination "black hole" start/end/precursor density: Recombination black hole start (*Bs*) and end (*Be*) points delineate the start and end of the heterochromatic centromeric region which has reduced DSB formation. Parameter *Bd* indicates the relative precursor density of the "black hole" and was set to 0.01 for all simulations (1 = no reduction in precursors, 0 = no precursor formation). Values were determined based on recombination frequencies observed in the backcross data (Table S1, Figure S1) and correspond to regions of the Arabidopsis genome with high DNA methylation, low H3K4me3, and reduced DSB formation (38).

Crossover Patterning Parameters:

Smax - Maximum stress level per bivalent: Crossovers are promoted at precursor sites by crossover promoting "stress" (*S*). *Smax* is maximum level of stress a bivalent is subject to during simulation. The biological correlate of the crossover promoting stress is not precisely defined but may relate to the expansion of chromatin during early prophase (8).

Bsmax – Similarity in maximum stress levels between bivalents: Bsmax sets the similarity of *Smax* between simulated bivalents and was set to be constant for all simulations (*Bsmax* = 1).

L_{BF} *– Stress relief distance:* The parameter L_{BF} corresponds to the length of the chromosomal interval over which a CO relieves stress i.e. stress-relief propagates out from COs a distance of ½ L_{BF} in either direction.

cL/R – Left and Right end clamping: In the beam-film model, "clamping" at chromosome ends determines how stress is supported in terminal regions. Unclamped chromosome ends (*cL* = 0; *cR* = 0) cannot support stress and so locally relieve stress, behaving as if there were a crossover

at the chromosome end. Clamped chromosome ends (cL = 1; cR = 1) experience stress as elsewhere along the bivalent.

T2Prob - Probability that a non-crossover designated precursor will form a Type II crossover: The parameter T2Prob defines the probability that a precursor site (i.e. DSB) not designated to become a class I crossover will become a class II crossover.

Maturation Parameter:

M – Crossover maturation efficiency: In the beam film model, it is possible to model failure of crossover maturation. If failure occurs, the CO-designated site inhibits nearby crossovers but does not itself develop into a crossover. We assumed 100% crossover maturation efficiency for all simulations (M = 1).

Double crossover class determination: The proportion of each class of DCO for a given inter-interval distance was determined from simulations modelling the formation of class I crossovers only (*T2Prob* = 0), class II crossovers only (*Smax* = 0), or both class I and II crossovers. For each simulation, numbers of DCOs were tallied for each inter-interval distance (IID, the distance between a pair of genetic intervals). For each IID, numbers of DCOs involving two class I COs (DCO_{I_I}), two class II COs (DCO_{II_II}) or all DCOs (DCO_{ALL}) were calculated from the respective simulations. $DCO_{I\_II} = DCO_{ALL} - (DCO_{I\_I} + DCO_{II\_II})$.

Response of model to parameters *L*, *Smax, T2Prob* and *N*: To investigate the response of the model to parameters *L*, *Smax* and *T2Prob* we simulated 30000 bivalents for an "idealized" male Arabidopsis chromosome (N = 60, B = 1, E = 0.6, Bs = 0.45, Be = 0.55, Bd = 0.01, *Smax*

= 9, *Bsmax* = 1, *A* = 1, *L* = 0.7, *cL* = 0.8, *cR* = 0.8, *M* = 1, *T2Prob* = 0.004) as described above, varying one specified parameter.

Data availability statement

Dataset S1 contains male and female genotyping data originally reported in Girault et al. (29). Dataset S2 contains male and female recombination location data. Code used for parameter optimization is available at https://github.com/andrewhmlloyd/BeamFilmBestFit.

RESULTS

Beam-Film simulations replicate CO patterning in Arabidopsis.

To determine the likely biological determinants of differences in crossover patterning between male and female meiosis, we compared beam-film parameter estimates obtained for the two sexes. To obtain these estimates, we ran a series of beam-film simulations using a broad range of parameter values and compared simulated recombination data to our experimental dataset. Independent simulations were run for each of the five Arabidopsis chromosomes for each sex. Parameter best-fits for each chromosome and sex were then obtained by comparing crossover number and distribution, and interference relationships (CoC curves) of simulated recombination and experimental data (Figure 1 & S1-2). Global parameter estimates were then derived for male and female meiosis by averaging the individual estimates of the five chromosomes (Figure 2). As parameter estimates for male and female are drawn from the same parameter space, the female best-fit simulations are an example of a parameter set that did not fit the male data and vice versa. Figure S3 shows several other examples.

Crossover Distribution: Simulated CO distributions using optimized parameter sets reproduced CO distributions observed in the experimental data. Simulations captured the broad

scale trends, rather than fine-scale differences in CO frequency. Highest recombination in males was found in distal regions and highest recombination in females in regions adjacent to the centromere (Figure 1, Figure S1). The exception was the short arms of chromosomes 2 and 4 in males which have high experimental recombination rates but had low levels of recombination when simulated using the global best-fit parameters (Figure S1). It is possible that this is related to the presence of nucleolar organizer regions (NORs) on the short arms of these two chromosomes, which are not explicitly modelled in simulations.

CoC curves: The coefficient of coincidence (CoC) is the ratio of the observed and expected numbers of double crossovers (DCOs) for a given pair of intervals, given the rates of single COs in the two intervals. When interference strength is high, CoC values tend to be low as there are fewer DCOs observed than expected. CoC shows a characteristic curve when plotted against inter-interval distance (Figure 1B-C), with low CoC for small inter-interval distances (when a CO in one interval suppresses the occurrence of a CO in the neighboring interval) and CoC approximating 1 for large inter-interval distances (over which the interference signal no longer spreads along the chromosomes). A useful measure when analyzing such curves is L_{CoC} (9), the inter-interval distance at which the observed number of double crossovers is half the expected number (CoC = 0.5, dashed line, Figure 1B-C). For all analyses the simulated data gave L_{CoC} values that were no different from those determined from the equivalent experimental data (Table 1.). For both experimental and simulated data, L_{CoC} was significantly smaller in males than in females if measured in Mb but showed no difference when measured in μm SC (Table 1, Figure 1 and Figure S2). This confirms that genetic measurements of interference (e.g. L_{CoC} in Mb) are lower in male than in female but suggests that the physical distance over which interference spreads (measured in μm SC) may be similar.

In the Beam film model, the CO patterning process is primarily determined by the strength of the (CO)-designation (*S*, *Smax*) and by the distance over which interference spreads (L_{BF}). We thus compared estimates of these two parameters between male and female meiosis.

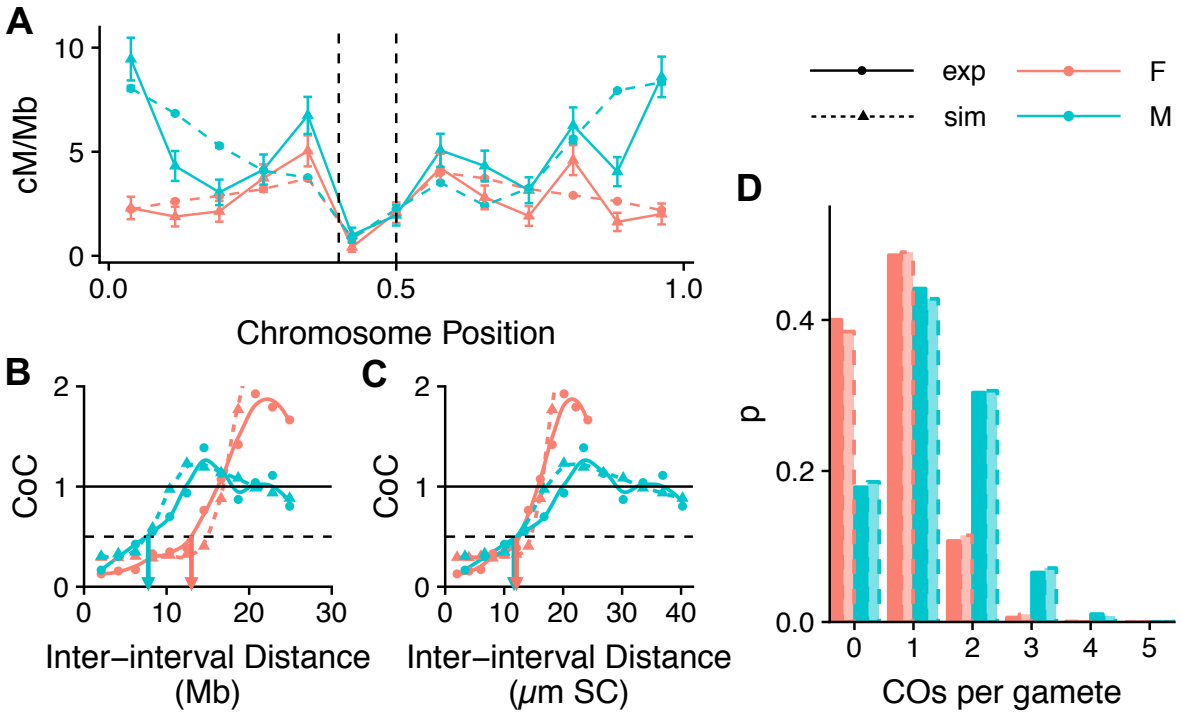

Figure 1. Crossover analysis for Arabidopsis chromosome 5. Each analysis includes experimental (solid lines) and simulated (dashed lines) data for male (blue) and female (orange). **A** Crossover distributions for Arabidopsis chromosome 5. Dashed lines represent the limits of the centromeric region over which precursor (DSB) number is markedly reduced both biologically (38) and during simulations. Error bars indicate 95% confidence intervals. **B-C** CoC curves for chromosome 5 with inter-interval distance (IID, the distance between a pair of genetic intervals) measured in Mb (**B**) or µm SC (**C**). L_{CoC} for male and female (blue and orange arrows respectively) differed when IIDs were measured in Mb but not when measured in µm SC. **D** Event distribution for chromosome 5. Male and female simulations shown, assume 250 DSBs genome-wide. Chromosomes were divided into 13 equal-sized adjacent intervals for analysis.

Estimates of crossover promoting "stress" are the same for male and female meiosis

In the beam-film model precursor (DSB) fate is determined by the crossover-promoting "stress" (*S*) experienced by that precursor as well as the precursor's sensitivity (a random value between 0-1, determined by parameter *A*, see methods). When simulating each bivalent, the value of *S* is progressively increased until *S* = *Smax,* with each precursor experiencing stress equal to the product of *S* and the precursor's sensitivity. At some point the stress experienced by the most sensitive precursor reaches the critical value of 1 and will undergo CO-designation. Stress-relief will then extend out from that position. As *S* increases to *Smax,* additional precursors usually experience sufficient stress to promote the designation of further COs, although in these subsequent rounds of crossover designation, the stress experienced by precursors is reduced by the sum of any stress-relief caused by interference from nearby COs. If Smax is set below 1 then no pre-cursor will achieve the critical stress value and therefore no class I crossovers will be designated.

According to this model, the higher the final maximum stress value (*Smax*), the more CO-designations. However, despite male having significantly more COs than female, the predicted levels of maximum stress for the five chromosomes were similar for both sexes: *Smax* - male 7 ± 1.9 and female 6.9 ± 0.7, $p = 1$ (Bonferroni corrected) (Figure 2, Table S1). Thus, our modelling suggests that increased crossover frequencies in male are not due to differences in the CO-designation driving force.

Interference propagates the same physical distance along male and female bivalents, but has a greater "effective" strength in female.

The parameter L_{BF} determines the length of the chromosomal region, centered on a crossover, over which stress is relieved by that crossover. In the beam-film model, the magnitude of the

stress-relief decreases exponentially with distance from the CO, such that there is maximal stress-relief immediately surrounding the CO and almost no stress-relief at a distance ½ L_{BF} in either direction from the CO (8, 9).

When running simulations L_{BF} is specified as the proportion of total chromosome length (i.e. chromosome length is set to 1), but is converted to length in Mb or μm SC to enable comparisons between chromosomes of different lengths. For some chromosomes, the estimated distance over which stress is relieved was greater than the length of the chromosome in question. While this may at first seem contradictory, it is in fact required if a CO suppresses the formation of additional COs more than half the length of the chromosome away. An example can be seen for chromosome 2 in females which has an estimated SC length of 16.2 μm and an estimated stress relief distance (L_{BF_SC}) of 25.9 μm. As can be seen from the CoC curve for this chromosome (Figure S2) it is clear that the observed number of DCOs are less than expected (i.e. CoC < 1) even when intervals are at opposite ends of the chromosome (e.g. inter-interval distance ~14 μm).

When measured in Mb (L_{BF_Mb}) the average best-fit estimates of stress relief distance were significantly higher in females: L_{BF_Mb} – male 17.1 ± 3.5 Mb and female 28.8 ± 3.1 Mb, p = 0.0095 Bonf. corr. (Figure 2, Table S1). However, when the distance metric was converted to μm SC (L_{BF_SC}), using the best available estimates of SC length in the two sexes (39), there was no-longer any difference in the estimated stress relief distance between the two sexes: L_{BF_SC} – male 27.7 ± 5.6 μm and female 23.7 ± 2.5 μm, p = 1 Bonf. corr. (Figure 2). These results indicate that the physical distance over which interference spreads is the same in both male and female, but that the effect of interference on patterns of inheritance is greater in female than it is in male. This is because the same physical distance (μm SC) covers a greater proportion of total chromosome length (Mb) in female.

These findings highlight a key distinction between different possible interpretations of interference that can be broadly defined as “mechanistic” and “effective”. For clarity we here define our use of these terms which we will use in the remainder of this manuscript: We use the term “interference” when speaking broadly of the phenomenon, we use “mechanistic interference” when referring specifically to interference as defined in the beam-film model i.e. the distance along the chromosome (measured in μm SC) that the interference signal propagates, and we use the term “effective interference” to refer to interference as measured genetically (e.g. CoC or gamma, calculated from genetic data and expressed in Mb). “Effective interference” can be influenced by stress relief distance (in μm SC), but is also affected by other factors like rates of class II crossovers and chromatin loop size (Mb per μm SC). Thus, although mechanistic interference is identical for male and female meiosis, effective interference is stronger in female, resulting in fewer interference sensitive class I COs in female.

Estimates of chromosome end tethering (*cL/R*) are the same for male and female meiosis

In addition to *Smax* and L_{BF}, several other beam-film parameters commonly vary within or between species, and might contribute to sex-specific patterns of crossover formation (9). The first of these we focused on was the effect of “clamping” or tethering of chromosome ends, which determines how stress is supported in terminal regions. A probable biological correlate is the tethering of telomere ends to the nuclear envelope. If a chromosome is clamped/tethered it can support crossover promoting stress. If unclamped, stress can dissipate from the loose chromosome end which, according to the beam-film model, would tend to suppress CO formation. As the interference signal (stress-relief) cannot come from beyond the end of the chromosome, recombination frequencies will tend to be highest in distal regions when chromosomes are clamped and there is more than one CO per bivalent. Total clamping

averages (*cL/R*) for male and female were calculated from the estimated values of *cL* and *cR* for each sex. Clamping values were variable between chromosomes but there was no significant difference between the average clamping values: *cL/cR* male 0.78 ± 0.16 and female 0.69 ± 0.13, p = 1 Bonf. corr. (Figure 2). Differences in chromosome-end tethering are therefore unlikely to contribute to sex-specific differences in crossover patterning.

Fewer class II crossovers occur through the female germline

The number of class II COs in a simulation is determined by parameter *N*, the number of recombination precursor sites (DSBs) and parameter *T2Prob* which specifies the probability of a non-crossover designated precursor site becoming a class II CO. Assuming the same number of DSBs in male and female, the estimated likelihood of precursors becoming a class II CO was significantly higher in male than female meiosis: *T2Prob* - 0.0063 ± 0.0010 and 0.0036 ± 0.0008 respectively (p = 0.026, Bonf. corrected, Table 1, Figure 2). As male and female meiosis have the same number of precursors (DSBs) in these analyses, males have a proportionately higher number of class II COs: 1.575 ± 0.5 and 0.9 ± 0.2 respectively (p = 0.026, Bonf. corrected). We also determined what proportion of the total number of crossovers occur via the class II pathway (i.e. $p = CO_{II} / (CO_I + CO_{II})$. These values were equivalent for the two sexes: 0.14 ± 0.02 male, 0.14 ± 0.03 female, p = 1 Bonf. corr. A lower probability of class II crossover formation in female may therefore, in addition to the decrease in class I crossovers described above, contribute to sex-specific crossover patterning in Arabidopsis.

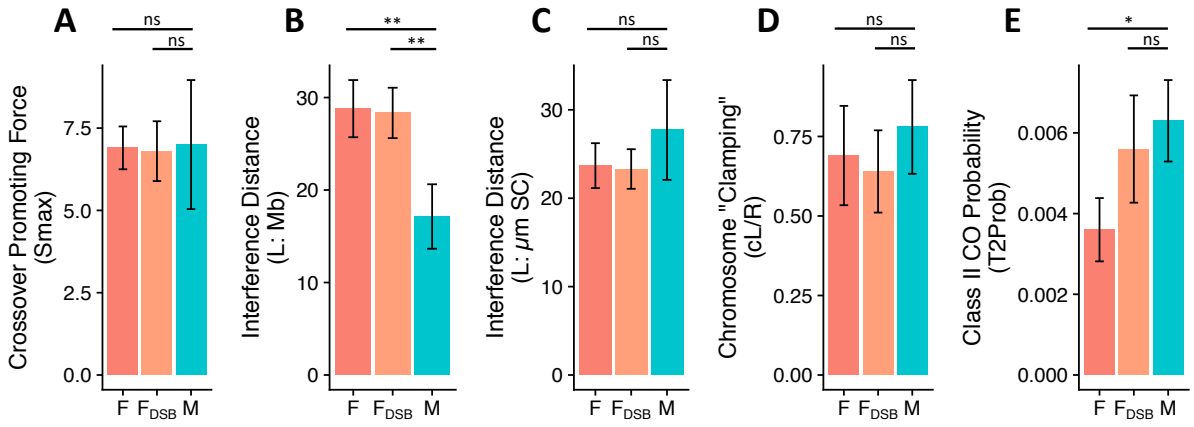

404

405 **Figure 2. Beam-film best-fit parameter estimates. A)** Estimates of crossover promoting force (*Smax*) were
406 identical for male and female with 250 DSBs (M and F respectively), and female with 150 DSBs (F_{DSB}).
407 Estimates of interference distance (L) were longer in male when measured in Mb (**B**) but not significantly
408 different when measured in μm SC (**C**). **D)** There was no significant difference in estimates of chromosome
409 clamping. **E)** The probability of non-class I-designated precursors becoming class II crossovers was
410 estimated to be lower in female than male if both sexes had 250 DSBs, but not significantly different if there
411 are reduced DSBs (150) in female. For each parameter and condition, the mean of the estimates for the five
412 chromosomes is shown. Error bars indicate 95% confidence interval. * $p < 0.05$, ** $p < 0.01$, after Bonferroni
413 multiple comparison correction.

414

415 **Fewer DSBs in female would explain lower class II CO numbers and unify estimates of**
416 **beam-film parameters for male and female meiosis.**

417 One of the parameters fixed for each round of analysis is the number of DSBs. While there are
418 relatively good estimates for the number of DSBs in male meiosis in Arabidopsis, cytological
419 analyses of female meiosis are more challenging and there are no reliable estimates of DSB
420 numbers. Thus, while we have assumed equal numbers of DSBs in male and female meiosis in
421 the analyses described above, it is possible that DSB numbers differ between the two sexes.
422 Meiotic DSBs occur in loop DNA that has been recruited to the chromosome axis (40). In
423 Arabidopsis female meiosis there are fewer (albeit larger) chromatin loops and the
424 chromosome axis is 40% smaller than in male meiosis (39) which could feasibly result in a

similar reduction in DSBs (31, 41). To understand whether reduced DSB numbers would have any effect on crossover patterning and/or estimates of parameter values in female meiosis, we repeated the best fit simulations assuming a reduction in DSBs equal to the reduction in SC length i.e. approx. 40% reduction, or 150 (rather than 250) DSBs per meiosis.

Optimized estimates of crossover promoting stress (*Smax*), interference strength / stress relief distance (L_{BF_Mb}, L_{BF_SC}) and chromosome tethering (*cL/cR*) were identical for both sets of simulations (F and $F_{DSB,}$ Figure 2). Estimates of class II crossover likelihood (*T2Prob*) were higher for simulations of female meiosis with reduced DSB numbers, and the optimized value no-longer differed from that estimated for male meiosis (Figure 2). Although the probability of class II CO formation was the same for male with 250 DSBs and female with 150 DSBs, the absolute number of class II crossovers was lower in female (due to the reduced number of DSBs): Male - 250 DSBs × *T2Prob* 0.0063 ± 0.001 = 1.58 ± 0.25; Female - 150 DSBs × *T2Prob* 0.0056 ± 0.001 = 0.90 ± 0.17 COs.

Table 1. L_{CoC} values

	Mb			µm SC		
	male	female	p value[#]	male	female	p value[#]
experimental	7.05 ± 0.50	12.84 ± 1.50	7.90E-07	11.65 ± 0.86	12.83 ± 1.50	1
simulated	6.30 ± 1.05	11.60 ± 0.83	1.40E-05	10.21 ± 1.75	11.20 ± 0.78	1
p value[#]	1	1		1	1	

[#] Bonferroni multiple-comparison corrected

Taken together, these results suggest that the smaller synaptonemal complex length in female, if accompanied by an equivalent reduction in DSBs, can account for all differences in crossover patterning between the two sexes, even if the mechanics of crossover patterning remain identical. The smaller SC in female accounts for stronger effective interference, and therefore

446 reduced crossovers, despite identical estimates of L_{BF_SC}. Similarly, a reduction in DSB density
447 (per Mb), due to the shorter SC, could account for the reduction in class II crossovers.
448
449 **Behavior of two-pathway beam-film model**
450 We next comprehensively explored the behavior of the two-pathway beam-film model, in order
451 to better understand how the patterning of class I and class II crossovers interact to influence
452 patterns of inheritance. To do this we simulated crossovers, independently varying the stress
453 relief distance ($L_{BF,}$ Figure 3A-C), crossover promoting stress (*Smax*, Figure 3D-F) and class
454 II CO probability (T2Prob, Figure 3G-I).
455
456 **COs tend to increase in regions adjacent to telomeres and pericentromeres**
457 Changes in L_{BF} and *Smax* dramatically altered CO distributions (Figure 3A & 3D) while
458 changing the proportion of class II COs had little effect (Figure 3G). Changes in CO frequency
459 were primarily observed in terminal regions (*Smax*, L_{BF}) and in regions adjacent to the peri-
460 centromere (L_{BF}) and showed increased CO frequencies with greater stress and decreased stress
461 relief distance (Figure 3A & 3D).
462
463 **L_{CoC} is primarily influenced by stress relief distance**
464 As has been observed previously in yeast (9) the parameter that most influenced CoC curves
465 was the stress relief distance (L_{BF}) with higher values of L_{BF} shifting CoC curves to the right.
466 Because of this shift, increases in L_{BF} resulted in proportional increases in $L_{CoC,}$ highlighting
467 that L_{CoC} (when measured in μm SC) is a useful proxy for stress relief distance. One major
468 advantage of L_{CoC} over L_{BF} is that it can be determined directly from experimental data without
469 the requirement for beam-film modelling and parameter optimization.

Intriguingly, behavior of CoC at small inter-interval distances differed from that observed at larger inter-interval distances. For example, an increase in the distance over which the interference signal is propagated would normally be expected to lead to lower values of CoC as more double crossovers are suppressed. However, at small inter-interval distances increased L_{BF} resulted in *increased* values of CoC (Figure 3C). It was also evident that while changes in the probability of class II CO formation had negligible effects on L_{CoC} and the shape of the CoC curve, it was the parameter that had the largest impact on CoC at small inter-interval distances (IID ~0.1, red lines, Figure 3I vs Figures 3C and 3F).

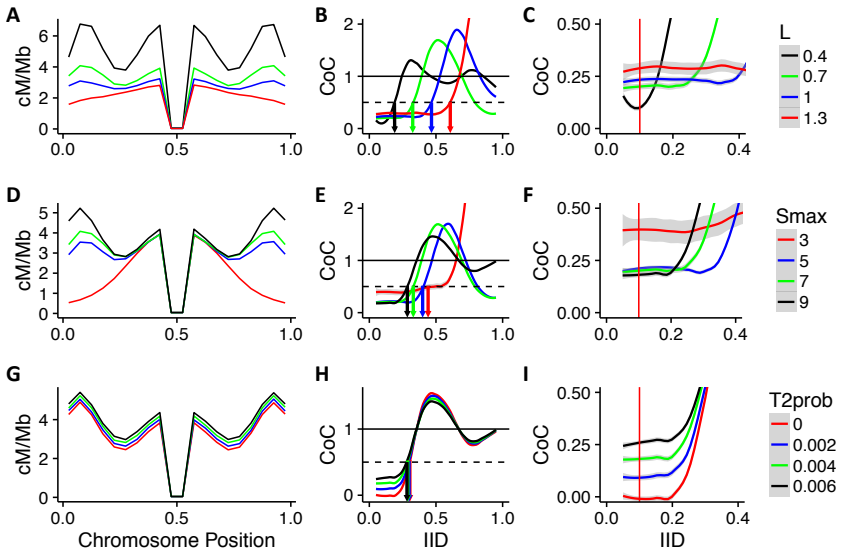

Figure 3. Effect of beam-film parameters on crossover patterning in Arabidopsis. The effect of altering a single beam film parameter – L (**A-C**), Smax (**D-F**) or T2Prob (**G-I**) – on crossover distribution (**A, D & G**) and CoC (**B-C**, **E-F** and **H-I**). Red vertical lines in **C**, **F** and **I** represent IID = 0.1. Grey shading in CoC curves indicate 95% confidence interval.

Differing classes of double COs at small and large IIDs cause opposite effects of altered stress relief distance on CoC: To further understand why CoC might behave differently at different inter-interval distances (IIDs), we sought to identify how changes in L_{BF} might differentially affect the expected and observed number of double COs (the determinants of

489 CoC) for different IIDs. Beam film simulations demonstrated that increased L_{BF} resulted in a
490 small decrease in the expected number of double COs (DCOs) for both small and large IIDs
491 (IID = 0.1 and 0.5; Figure 4A). This was anticipated given that the expected number of DCOs
492 for a pair of intervals is based purely on the respective rates of COs in the two intervals. In
493 contrast, the observed number of DCOs changed dramatically for IID = 0.5, but only
494 marginally for IID = 0.1 (Figure 4A) in response to changes in L_{BF}. As a result, CoC
495 dramatically decreased for IID = 0.5 with increased L_{BF} but increased slightly for IID = 0.1
496 (Figure 4B).
497
498 We reasoned that the difference in behavior might be due to the nature of the DCOs formed at
499 smaller and larger IIDs which might differ in their sensitivity to interference. For example,
500 DCOs can occur between two class I COs, two class II COs or between a class I and a class II
501 CO but interference only directly suppresses those involving two class I COs. We therefore ran
502 beam film simulations with class I COs only (*T2Prob* = 0), class II COs only (*Smax* = 0), or
503 both class I and class II COs and determined numbers of the different classes of DCOs formed
504 for each set of simulations at different IIDs (Figure 4C). From these numbers we determined
505 the proportions of the different classes of DCOs (Figure 4D) that occur for different IIDs under
506 standard conditions (i.e. when simulating both class I and class II COs). For small IIDs DCOs
507 are almost exclusively formed between a class I CO and a class II CO (Figure 4D). In contrast,
508 for larger IIDs (≥ 0.4) the majority of DCOs are formed between two class I COs (Figure 4D).
509 Cytological observations in tomato reporting the same phenomenon (42) suggest this is a
510 general feature of meiosis. As interference only suppresses DCOs involving two class I COs,
511 changes in L_{BF} will only directly affect DCO formation at larger IIDs. This pattern holds when
512 the proportion of class II crossovers falls within the range normally observed (5-20%), although

when class II crossovers are absent or make up the majority of crossovers then most DCOs involve two class I or two class II COs respectively for all IIDs (Figure S4).

Both the expected number of DCOs and observed DCOs at small IIDs are indirectly affected by increased L_{BF} due to the associated decrease in the frequency of class I COs. The magnitude of the change is greater for the expected number of DCOs, which can be seen from the equations below. Here *CI* and *CII* are the rates of class I and class II crossovers respectively in the two intervals:

$$\mathrm{DCO}_{exp} = (CI_{Int1} + CII_{Int1}) \times (CI_{Int2} + CII_{Int2})$$

$$\mathrm{DCO}_{obs_{Small\_IID}} \sim (CI_{Int1} \times CII_{Int2}) + (CI_{Int2} \times CII_{Int1})$$

For small IIDs, while *CI* >> *CII,* the reduction in the expected number of DCOs is approximately twice that of the observed reduction in DCOs, resulting in an increase in CoC.

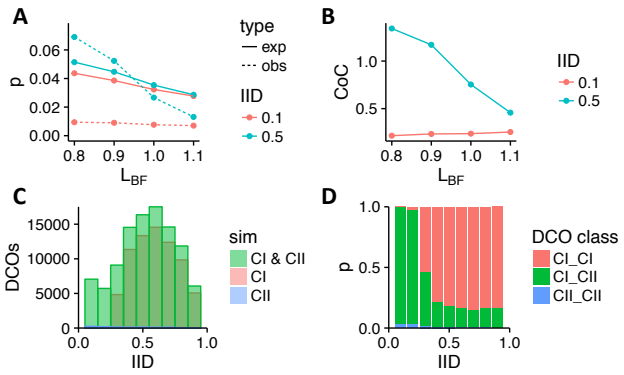

Figure 4. Influence of IID on CoC response to changes in L_{BF}. A The expected (solid line) and observed (dashed line) proportion of interval pairs receiving a double crossover (DCO) for two different inter-interval distances (IIDs); calculated from simulations with varying values of L_{BF}. **B** CoC values for two IIDs calculated from simulations with varying values of L_{BF}. **C** The number of DCOs observed for different IIDs from simulations involving class I and class II crossovers (CI & CII), class I crossovers only (CI) or class II

crossovers only (CII). **D** The proportions of DCOs formed between two class I crossovers (CI_CI), two class II crossovers (CII_CII), or a class I and a class II CO (CI_CII) for different IIDs.

Crossover homeostasis is influenced by the proportion of class II COs:

Finally, we assessed the effects of the rate of class II crossover formation on crossover homoeostasis. Crossover homoeostasis maintains crossover number despite differences in DSB formation (43–45). As described above, we observed few changes in crossover number and estimates of beam-film parameters when we modelled a 40% decrease in DSB numbers, the beam-film model therefore displays strong CO homeostasis when modelling wild type Arabidopsis meiosis. We reasoned however, that if the proportion of class II crossovers increased, such as is seen in some mutant contexts (e.g. 34), then DSB number should have a greater influence on the number of crossovers.

When modelling wild type meiosis, altered DSB number had relatively little effect on crossover distributions or CoC curves (Figure 5A-B). For CO distribution, increased DSBs resulted in a slight increase in proximal and distal crossovers, but fewer interstitial crossovers. The only clear difference in CoC was for small inter-interval distances, where higher DSB numbers resulted in higher values of CoC (Figure 5C). In contrast, altering the number of DSBs in a context where a high proportion become class II crossovers had a dramatic effect on crossover patterning. Here increased DSBs resulted in proportionate increases in crossovers (Figure 5D). Regardless of the number of DSBs, CoC values were approximately 1 for all inter-interval distances (Figure 5E-F).

We next modelled how DSB number affects the total number of crossovers for male and female meiosis in both contexts. In wild type, doubling the number of DSBs resulted in a ~ 15% increase in crossovers in male and female (Figure 5G). In a context with a high number of class II crossovers, doubling the number of DSBs resulted in almost doubling the number of

crossovers (Figure 5G). The number of DSBs has often been reported to have limited influence on rates of crossovers due to crossover homeostasis (43–45). Our results indicate that the number of DSBs primarily affects the number of COs when the proportion of class II crossovers is high, and by extension suggests that the probability of class II CO formation has a major influence on crossover homeostasis.

For a given number of DSBs the modelling predicts ~ 65% more crossovers in wild type male than wild type female, but essentially equal numbers of crossovers when the probability of class II crossovers is high (Figure 5G).

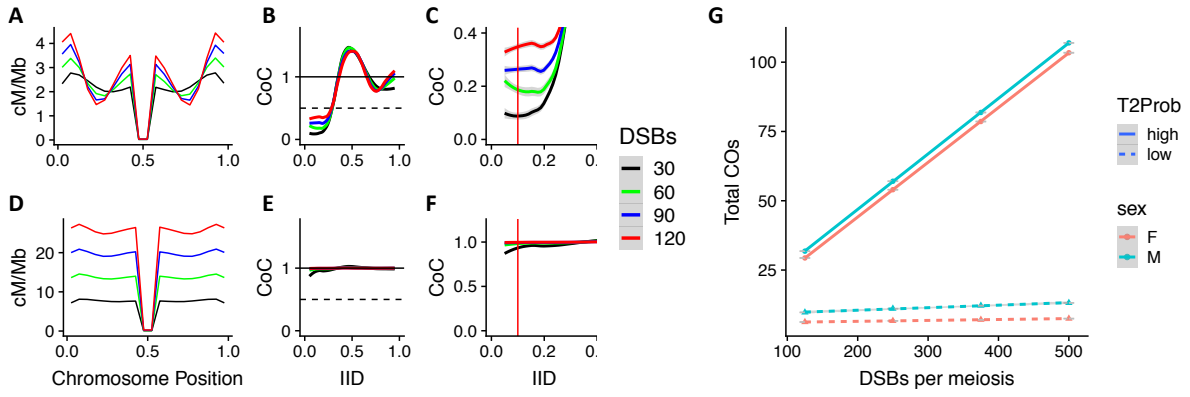

Figure 5. Influence of DSB number on crossover patterning and homoeostasis is dependent on the probability of class II crossovers. A-C show results for simulations of wild type meiosis, **D-F** show results for simulation of meiosis with increased class II crossover formation (T2Prob). **A**) Increased DSBs in wild type resulted in more proximal and distal crossovers, but fewer interstitial crossovers. **D**) In mutants with increased class II crossovers, more DSBs resulted in a uniform increase in crossovers. **B-C**) For wild type , CoC values increased at small inter-interval distances with increased DSBs. **E-F**) With increased class II COs, CoC values were ~1 for all inter-interval distances and all DSB numbers. **(G)** Total crossover number for genome-wide simulations using best-fit parameters for male and female meiosis and varying numbers of DSBs. In wild type (dashed lines) increasing DSBs had a minimal effect on total crossovers. With increased class II COs (solid lines) doubling DSBs resulted in twice as many crossovers. Grey shading in CoC curves indicates 95% confidence interval.

582

583 **DISCUSSION**

584 Crossover interference is a well-known genetic phenomenon; however, its mechanistic basis is
585 only just now coming to light. The interference signal is thought to propagate a set physical
586 distance ($L_{BF,}$ usually measured in μm SC) from designated crossover sites (4, 9), and analyses
587 commonly use cytological observations and simulations of class I crossover positions along
588 the length of a synapsed bivalent (4, 9).

589

590 To gain insights into the differences between female and male meiosis in Arabidopsis, we
591 analyzed a large Arabidopsis reciprocal backcross data set (29) and performed two-pathway
592 (i.e. both class I and class II COs) beam film best-fit simulations. Our modelling suggests that
593 the major differences in crossover number, crossover distribution and interference relationships
594 between the sexes can all be explained by the observed difference in SC length between male
595 and female meiosis. The relationship between genome size and SC length is governed by the
596 size/number of chromatin loops, which occur at a conserved density of ~20 per μm SC across
597 a wide range of organisms (46). As genome size is identical for both sexes in Arabidopsis, we
598 would expect loop size in male meiocytes to be about 60% of that found in female meiocytes.
599 Exactly how chromatin loop size is determined remains unclear but this decision occurs very
600 early in, or prior to, meiosis (3, 47). It is probable, therefore, that the cause of differences in
601 crossover patterning also occurs very early in, or prior to, meiosis. Interestingly humans also
602 display a sex-specific differences in chromatin loop-size and SC length, although in this case
603 female meiocytes have shorter loop-size, longer SC and more crossovers (48).

604

605 It has been reported previously that effective crossover interference is stronger in females than
606 in males in Arabidopsis (35). Our analyses indicate that the interference signal is propagated

607 over the same physical distance (μm SC) in both male and female meiosis, and thus from a
608 mechanistic standpoint interference is identical in the two sexes. The higher *effective*
609 interference (i.e. the effect on the inheritance of two linked genetic loci) observed in females
610 can be entirely explained by the difference in SC length between the two sexes, as a given
611 distance in μm SC corresponds to a greater length in Mb. It is worth noting that our estimates
612 of L_{BF} for male (27.7 ± 5.6 μm) and female (23.7 ± 2.5 μm) Arabidopsis are similar to estimates
613 for tomato (14 μm, ref 9) but are 80 to 90-fold larger than for yeast (0.3 μm, ref 9). This vast
614 difference in the distance across which interference propagates in different taxa, as estimated
615 by the beam-film model, remains challenging to explain biologically.
616
617 In addition to explaining differences in effective interference, SC length also explained the
618 differences in CO distribution observed between the sexes. In male meiosis, crossovers are
619 high adjacent to the peri-centromeres and in the distal regions, while in female meiosis
620 crossovers are high adjacent to the peri-centromeres but low in the distal regions (29, 39). Our
621 modelling shows that increases in the proportion of the chromosome over which interference
622 spreads (either through a reduction in SC length, or an increase in L_{BF}) reduces crossovers
623 particularly in distal regions. The lower SC length in females can therefore account for the
624 observed differences in crossover distribution.
625
626 In mammals, SC length is correlated with the number of DSBs (31, 41, 49). If the same holds
627 true in plants, then we might expect fewer DSBs in female meiosis. Our analysis revealed that
628 while the number of DSBs had very little influence on crossover distributions and CoC curves,
629 a decrease in the number of DSBs resulted in an increase in the estimated proportion of DSB
630 sites that become class II crossovers (*T2Prob*). Thus, the reduction in SC length observed for
631 females, if accompanied by an equivalent reduction in DSBs, can also account for proposed

differences in the number of class II crossovers between male and female meiosis. At least one line of evidence suggests this question may not be fully resolved however. In mutant lines with large numbers of additional class II crossovers, the recombination landscape of male and female meiosis are roughly equivalent with even a slightly higher number of crossovers in female (34). This suggests the possibility of similar numbers of DSBs in male and female meiosis. Further comparative cytological studies of male and female meiosis will be required to fully answer these questions, for example it would be interesting to see if SC lengths still differ between male and female in these mutant contexts.

Given the substantial differences in crossover patterning between female and male meiosis it is striking that they can all be accounted for by the difference in SC length. It is similarly striking that despite the differences in crossover patterning there are also no significant differences between the sexes in the estimated beam-film model parameters (if L is expressed in μM SC, and the number of DSBs is reduced in line with the shorter SC in female). This gives us good confidence in our approach, and suggests that similar investigations, in different contexts (e.g. mutants, over expression lines, environmental conditions), could provide further mechanistic insights into the factors governing crossover patterning in Arabidopsis.

When exploring the impact of varying the beam-film parameters it was clear that increased crossover promoting stress (*Smax*) or decreased stress relief distance (L_{BF}) resulted in increased crossovers particularly in terminal regions. Crossovers also increased in proximal regions but only when the stress relief distance was low and so were not suppressed by the increase in terminal crossovers (e.g. Figure 3A – L 0.4 compared to Figure 3A – L > 0.5 and Figure 3D). This is explained in the beam-film model, by the fact that additional crossovers will tend to occur in regions that experience, on average, less stress relief. Additional crossovers in terminal

regions are only suppressed by prior crossovers in one direction i.e. crossovers located toward the centromere, in contrast additional crossovers in interstitial regions are suppressed by both distal and proximal crossovers (Figure 6). Similarly, the low precursor density at the centromere results in fewer crossovers and thus regions adjacent to the centromere experience less stress relief than interstitial regions (Figure 6), resulting in more crossovers. This is particularly true when the stress relief distance is low, and the local environment has greater effect (e.g. Figure 3A).

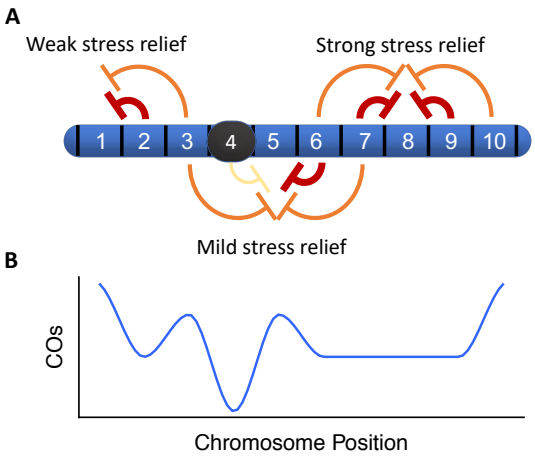

Figure 6. COs formed after the initial obligatory CO tend to accumulate in terminal and proximal regions. A) Terminal regions (e.g. interval 1) experience weaker stress relief than interstitial regions (e.g. interval 8) as they are surrounded by fewer crossovers. Similarly, proximal regions (e.g. interval 5) experience less stress relief, due to the lower precursor number and therefore fewer COs in centromeric regions (interval 4). **B)** After designation of the first crossover (which will not be influenced by interference/stress relief), additional crossovers tend to accumulate in terminal and proximal regions due to their lower average levels of stress relief.

In addition to mechanistic insights into the factors governing crossover patterning in Arabidopsis, the model can be used to make predictions about how important agricultural goals such as heightened recombination rates could be achieved. For example, with the development of CRISPR and related technologies, it is possible to modulate the number or location of DSBs in early meiosis and there is interest in using this approach to alter recombination rates in plant breeding programs (50–52). In most organisms, crossover numbers are thought to be maintained independently from the number of DSBs through crossover homeostasis (43–45). Our modelling suggests that the extent to which homoeostasis maintains crossover numbers is determined by the proportion of DSBs that become class II crossovers: The higher the proportion of class II crossovers, the more DSB number will affect crossover number. Thus, we predict that combining the knock out of class II CO suppressing proteins (e.g. RECQ4, FANCM, FIGL1, 53–55) with approaches to increase meiotic DSBs could maximize increases in recombination and the associated benefit to breeding programs.

One of the surprising findings of our analysis is that for small inter-interval distances, an increase in the distance over which the interference signal is propagated can result in increased values of CoC (Figure 3) i.e. decreased effective interference. This behavior is not specific to the beam-film model but is expected whenever both class I and class II crossovers occur, and there is a change in the strength of suppression of closely spaced class I crossovers. This finding highlights the need for caution when interpreting interference data and particularly in the distinction between mechanistic (e.g. L_{BF}) and effective (e.g. CoC from genetic data) measurements of interference. It should also be noted that at small inter-interval distances the magnitude of the predicted change in CoC is small, and that for specific interval pairs the effect of the local chromosomal landscape (e.g. recombination hotspots etc) may out-weigh the effect predicted by the model. Despite these caveats, it is clear that an increase or decrease in

mechanistic interference strength (L_{BF}) is not expected to result in an equivalent increase or decrease respectively in *effective* interference for small IIDs. Given the widespread use of reporter lines that determine recombination rates and CoC values for closely linked intervals (56) it is important to realize that these lines may give little to no insight into any change in the mechanics of crossover interference.

As an example, two recent papers investigated altered recombination rates at temperature extremes in Arabidopsis (57, 58). In both cases, increased temperature gave rise to more class I COs, but the increased COs were associated with no change, or a decrease in genetic measurements of CoC (i.e. effective interference). In the studies, CoC (or interference ratio) was measured by tracking the inheritance of closely linked fluorescent reporter genes in pollen, and thus combined both class I and class II crossovers measured at a small inter-interval distance. While it could be concluded from these studies that temperature increases class I crossovers without any effect on interference, these results are also consistent with an alternative hypothesis i.e. that increased temperature decreases the distance over which interference is propagated, resulting in increased class I COs, but with no effect on genetic measurements of interference at small-inter-interval distances. Or to put it another way, high temperature might decrease *mechanistic* interference, but result in an increase (or no change) in *effective* interference for small IIDs. There is good evidence that heightened temperature might have such a mechanistic effect, given that the chromosome axis is thought to mediate interference (3) and the synaptonemal complex / axis structure is sensitive to temperature (59, 60) but this remains to be experimentally validated.

While the beam-film model was able to reliably model genetic recombination data, there are several ways in which models of crossover patterning might further be improved with increased

726 understanding of the underlying biology. For example, when calculating L_{BF} and L_{CoC} in µm
727 SC using back-cross data, we assume a direct relationship between SC length and Mb. In
728 Arabidopsis the relationship between SC length and Mb is constant between whole
729 chromosomes (R^2 = 0.99, based on data from (61)), however the relationship may not be
730 constant within a chromosome (62). Establishing how the relationship between Mb and µm SC
731 changes for different chromosomal domains would provide one means to improve models of
732 crossover patterning when using genetic data. Another question is whether DSB density is
733 constant along the length of the chromosome? If so, is it constant relative to SC length or length
734 in Mb? Recently Spo11-oligo sequencing has demonstrated relatively constant DSB formation
735 along the length of the chromosome, although there are clearly regions of higher and lower
736 DSB density, particularly the centromeres where DSB formation is strongly suppressed (38).
737 It would be interesting to incorporate such data into future models of crossover patterning.
738
739 Despite these possible improvements to future models, it is clear that we can gain novel insights
740 into crossover patterning using genetic recombination data in combination with beam-film
741 simulations. These are particularly powerful when, as for this study, we have good estimates
742 of SC length for all chromosomes, circumventing the need for cytological determination of
743 crossover locations. This enables us to take advantage of the main benefit of genetic data, that
744 it incorporates all crossover events, and thus enables us to develop a more nuanced
745 understanding of the interplay between the mechanistic determinants of crossover-interference
746 and the final effect on patterns of inheritance.
747

748 **ACKNOWLEDGEMENTS**

749 We thank Christine Mezard for providing the experimental Arabidopsis recombination dataset
750 and for critical reading of the manuscript. A.L. was funded by a Marie Curie fellowship (PIOF-

751 GA-2013-628128) and the European Union's Horizon 2020 research and innovation program
752 under the Marie Skłodowska-Curie grant agreement No 663830. The IJPB benefits from the
753 support of the LabEx Saclay Plant Sciences-SPS (ANR-10-LABX-0040-SPS).

REFERENCES

1. Sturtevant AH (1915) The behavior of the chromosomes as studied through linkage. *Z Indukt Abstamm Vererbungsl* 13:234–287.
2. Muller HJ (1916) The Mechanism of Crossing-Over . II. *Am Nat* 50:284–305.
3. Zickler D, Kleckner N (2015) Recombination, pairing, and synapsis of homologs during meiosis. *Cold Spring Harb Perspect Biol* 7:a016626.
4. Zhang L, et al. (2014) Topoisomerase II mediates meiotic crossover interference. *Nature*:18–20.
5. Mcpeek MS, Speed TP (1995) Modeling Interference in Genetic Recombination. 139:1031–1044.
6. Housworth EA, Stahl FW (2003) Crossover Interference in Humans. 188–197.
7. Broman KW, Weber JL (2000) Characterization of Human Crossover Interference. 1911–1926.
8. Kleckner N, et al. (2004) A mechanical basis for chromosome function. *Proc Natl Acad Sci* 101:12592–12597.
9. Zhang L, Liang Z, Hutchinson J, Kleckner N (2014) Crossover patterning by the beam-film model: analysis and implications. *PLoS Genet* 10:e1004042.
10. Sym M, Engebrecht J, Roeder GS (1993) ZIP1 is a synaptonemal complex protein required for meiotic chromosome synapsis. *Cell* 72:365–378.
11. Chua PR, Roeder GS (1998) Zip2, a Meiosis-Specific Protein Required for the Initiation of Chromosome Synapsis. *Cell* 93:349–359.
12. Agarwal S, Roeder GS (2000) Zip3 provides a link between recombination enzymes and synaptonemal complex proteins. *Cell* 102:245–255.
13. Tsubouchi T, Zhao H, Roeder GS (2006) The Meiosis-Specific Zip4 Protein Regulates Crossover Distribution by Promoting Synaptonemal Complex Formation Together

779 with Zip2. *Dev Cell* 10:809–819.
780 14. Hollingsworth NM, Ponte L, Halsey C (1995) MSH5, a novel MutS homolog,
781 facilitates meiotic reciprocal recombination between homologs in Saccharomyces
782 cerevisiae but not mismatch repair. *Genes Dev* 9:1728–1739.
783 15. Ross-Macdonald P, Roeder GS (1994) Mutation of a meiosis-specific MutS homolog
784 decreases crossing over but not mismatch correction. *Cell* 79:1069–1080.
785 16. Nakagawa T, Ogawa H (1999) The Saccharomyces cerevisiae MER3 gene, encoding a
786 novel helicase-like protein, is required for crossover control in meiosis. *EMBO J*
787 18:5714–5723.
788 17. Lynn A, Soucek R, Börner GV (2007) ZMM proteins during meiosis : Crossover
789 artists at work. *Chromosom Res* 15:591–605.
790 18. Lhuissier FGP, Offenberg HH, Wittich PE, Vischer NOE, Heyting C (2007) The
791 Mismatch Repair Protein MLH1 Marks a Subset of Strongly Interfering Crossovers in
792 Tomato. *Plant Cell Online* 19:862–876.
793 19. Chelysheva L, et al. (2012) The Arabidopsis HEI10 is a new ZMM protein related to
794 Zip3. *PLoS Genet* 8:e1002799.
795 20. Hollingsworth NM, Brill SJ (2004) The Mus81 solution to resolution: Generating
796 meiotic crossovers without Holliday junctions. *Genes Dev* 18:117–125.
797 21. Kurzbauer M-T, et al. (2018) Arabidopsis thaliana FANCD2 Promotes Meiotic
798 Crossover Formation. *Plant Cell* 30:tpc.00745.2017.
799 22. Mercier R, et al. (2005) Two Meiotic Crossover Classes Cohabit in Arabidopsis : One
800 Is Dependent on MER3 , whereas the Other One Is Not. *Curr Biol* 15:692–701.
801 23. Cooper TJ, Crawford MR, Hunt LJ, Llorente B (2018) Mismatch repair impedes
802 meiotic crossover interference.
803 24. Falque M, Anderson LK, Stack SM, Gauthier F, Martin OC (2009) Two Types of

804 Meiotic Crossovers Coexist in Maize. *Plant Cell* 21:3915–3925.
805 25. White MA, Wang S, Zhang L, Kleckner N (2017) Quantitative Modeling and
806 Automated Analysis of Meiotic Recombination. *Meiosis*, ed Stuart DT (Springer New
807 York, New York, NY), pp 305–323.
808 26. Wang S, Zickler D, Kleckner N, Zhang L (2015) Meiotic crossover patterns:
809 Obligatory crossover, interference and homeostasis in a single process. *Cell Cycle*
810 14:305–314.
811 27. Loidl J (2016) Conservation and Variability of Meiosis Across the Eukaryotes. *Annu*
812 *Rev Genet* 50:293–316.
813 28. Mercier R, Mezard C, Jenczewski E, Macaisne N, Grelon M (2014) The Molecular
814 Biology of Meiosis in Plants. *Annu Rev Plant Biol* 66:1–31.
815 29. Giraut L, et al. (2011) Genome-wide crossover distribution in Arabidopsis thaliana
816 meiosis reveals sex-specific patterns along chromosomes. *PLoS Genet* 7:e1002354.
817 30. Singer A, et al. (2002) 34. Sex-Specific Recombination Rates in Zebrafish (Danio
818 rerio).pdf. 657:649–657.
819 31. Gruhn JR, Rubio C, Broman KW, Hunt PA, Hassold T (2013) Cytological studies of
820 human meiosis: Sex-specific differences in recombination originate at, or prior to,
821 establishment of double-strand breaks. *PLoS One* 8:1–15.
822 32. Tortereau F, et al. (2012) A high density recombination map of the pig reveals a
823 correlation between sex-specific recombination and GC content. *BMC Genomics* 13.
824 doi:10.1186/1471-2164-13-586.
825 33. Phillips D, et al. (2015) The effect of temperature on the male and female
826 recombination landscape of barley. *New Phytol* 208:421–429.
827 34. Fernandes JB, Seguéla-Arnaud M, Larchevêque C, Lloyd AH, Mercier R (2017)
828 Unleashing meiotic crossovers in hybrid plants. *Proc Natl Acad Sci*:201713078.

829 35. Basu-roy S, Gauthier F, Giraut L, Mézard C (2013) Hot Regions of Noninterfering
830 Crossovers Coexist with a Nonuniformly Interfering Pathway in. *Genetics* 195:769–
831 779.
832 36. White MA, Wang S, Zhang L, Kleckner N (2017) Quantitative Modeling and
833 Automated Analysis of Meiotic Recombination. *Methods Mol Biol* 1471:305–323.
834 37. Berchowitz LE, Copenhaver GP (2010) Genetic interference: don't stand so close to
835 me. *Curr Genomics* 11:91–102.
836 38. Choi K, et al. (2018) Nucleosomes and DNA methylation shape meiotic DSB
837 frequency in Arabidopsis thaliana transposons and gene regulatory regions. *Genome*
838 *Res* 28:1–15.
839 39. Drouaud J, et al. (2007) Sex-specific crossover distributions and variations in
840 interference level along Arabidopsis thaliana chromosome 4. *PLoS Genet* 3:e106.
841 40. Panizza S, et al. (2011) Spo11-accessory proteins link double-strand break sites to the
842 chromosome axis in early meiotic recombination. *Cell* 146:372–83.
843 41. Baier B, Hunt P, Broman KW, Hassold T (2014) Variation in Genome-Wide Levels of
844 Meiotic Recombination Is Established at the Onset of Prophase in Mammalian Males.
845 *PLoS Genet* 10. doi:10.1371/journal.pgen.1004125.
846 42. Anderson LK, et al. (2014) Combined fluorescent and electron microscopic imaging
847 unveils the specific properties of two classes of meiotic crossovers. *Proc Natl Acad Sci*
848 *U S A* 111:13415–13420.
849 43. Cole F, et al. (2012) Homeostatic control of recombination is implemented
850 progressively in mouse meiosis. *Nat Cell Biol* 14:424.
851 44. Martini E, Diaz RL, Hunter N, Keeney S (2006) Crossover Homeostasis in Yeast
852 Meiosis. *Cell* 126:285–295.
853 45. Rosu S, Libuda DE, Villeneuve AM (2011) Robust crossover assurance and regulated

854 interhomolog access maintain meiotic crossover number. *Science* 334:1286–9.
855 46. Zickler D, Kleckner N (1999) Integrating Structure and Function. *Annu Rev Genet*
856 33:603–754.
857 47. Kaiser VB, Semple CA (2018) Chromatin loop anchors are associated with genome
858 instability in cancer and recombination hotspots in the germline. *Genome Biol* 19:1–
859 14.
860 48. Tease C, Hultén MA (2004) Inter-sex variation in synaptonemal complex lengths
861 largely determine the different recombination rates in male and female germ cells.
862 *Cytogenet Genome Res* 107:208–215.
863 49. Ruiz-Herrera A, et al. (2017) Recombination correlates with synaptonemal complex
864 length and chromatin loop size in bovids—insights into mammalian meiotic
865 chromosomal organization. *Chromosoma* 126:615–631.
866 50. Puchta H (2017) Applying CRISPR/Cas for genome engineering in plants: the best is
867 yet to come. *Curr Opin Plant Biol* 36:1–8.
868 51. Hayut SF, Bessudo CM, Levy AA (2017) Targeted recombination between
869 homologous chromosomes for precise breeding in tomato. *Nat Commun* 8:1–9.
870 52. Choi K (2017) Advances towards Controlling Meiotic Recombination for Plant
871 Breeding. *Mol Cells* 40:814–822.
872 53. Crismani W, et al. (2012) FANCM Limits Meiotic Crossovers. *Science* 336:1588–
873 1590.
874 54. Seguela-Arnaud M, et al. (2015) Multiple mechanisms limit meiotic crossovers : TOP3
875 α and two BLM homologs antagonize crossovers in parallel to FANCM. 112.
876 doi:10.1073/pnas.1423107112.
877 55. Girard C, et al. (2015) AAA-ATPase FIDGETIN-LIKE 1 and Helicase FANCM
878 Antagonize Meiotic Crossovers by Distinct Mechanisms. *PLOS Genet* 11:e1005369.

879 56. Francis KE, et al. (2007) Pollen tetrad-based visual assay for meiotic recombination in
880 Arabidopsis. *Proc Natl Acad Sci U S A* 104:3913–8.
881 57. Lloyd A, Morgan C, Franklin C, Bomblies K (2018) Plasticity of meiotic
882 recombination rates in response to temperature in Arabidopsis.
883 58. Modliszewski JL, et al. (2018) Elevated temperature increases meiotic crossover
884 frequency via the interfering (Type I) pathway in Arabidopsis thaliana. *PLoS Genet*
885 14:1–15.
886 59. Loidl J (1989) Effects of elevated temperature on meiotic chromosome synapsis in
887 Allium ursinum. *Chromosoma* 97:449–458.
888 60. Morgan CH, Zhang H, Bomblies K (2017) Are the effects of elevated temperature on
889 meiotic recombination and thermotolerance linked via the axis and synaptonemal
890 complex? *Philos Trans R Soc B Biol Sci* 372. doi:10.1098/rstb.2016.0470.
891 61. López E, Pradillo M, Romero C, Santos JL, Cuñado N (2008) Pairing and synapsis in
892 wild type Arabidopsis thaliana. *Chromosom Res* 16:701–708.
893 62. Bickmore WA, Oghene K (1996) Visualizing the spatial relationships between defined
894 DNA sequences and the axial region of extracted metaphase chromosomes. *Cell*
895 84:95–104.
896

Figure 1. Crossover analysis for Arabidopsis chromosome 5. Each analysis includes experimental (solid lines) and simulated (dashed lines) data for male (blue) and female (orange). **A** Crossover distributions for Arabidopsis chromosome 5. Dashed lines represent the limits of the centromeric region over which precursor (DSB) number is markedly reduced both biologically (38) and during simulations. Error bars indicate 95% confidence intervals. **B-C** CoC curves for chromosome 5 with inter-interval distance (IID, the distance between a pair of genetic intervals) measured in Mb (**B**) or μm SC (**C**). L_{CoC} for male and female (blue and orange arrows respectively) differed when IIDs were measured in Mb but not when measured in μm SC. **D** Event distribution for chromosome 5. Male and female simulations shown, assume 250 DSBs genome-wide. Chromosomes were divided into 13 equal-sized adjacent intervals for analysis.

Figure 2. Beam-film best-fit parameter estimates. A) Estimates of crossover promoting force (*Smax*) were identical for male and female with 250 DSBs (M and F respectively), and female with 150 DSBs (F_{DSB}). Estimates of interference distance (L) were longer in male when measured in Mb (**B**) but not significantly different when measured in μm SC (**C**). **D)** There was no significant difference in estimates of chromosome clamping. **E)** The probability of non-class I-designated precursors becoming class II crossovers was estimated to be lower in female than male if both sexes had 250 DSBs, but not significantly different if there are reduced DSBs (150) in female. For each parameter and condition, the mean of the estimates for the five chromosomes is shown. Error bars indicate 95% confidence interval. * $p < 0.05$, ** $p < 0.01$, after Bonferroni multiple comparison correction.

Figure 3. Effect of beam-film parameters on crossover patterning in Arabidopsis. The effect of altering a single beam film parameter – L (**A-C**), Smax (**D-F**) or T2Prob (**G-I**) – on crossover distribution (**A, D & G**) and CoC (**B-C**, **E-F** and **H-I**). Red vertical lines in **C**, **F** and **I** represent IID = 0.1. Grey shading in CoC curves indicate 95% confidence interval.

925 **Figure 4. Influence of IID on CoC response to changes in L_{BF}.** **A** The expected (solid line)
926 and observed (dashed line) proportion of interval pairs receiving a double crossover (DCO) for
927 two different inter-interval distances (IIDs); calculated from simulations with varying values
928 of L_{BF}. **B** CoC values for two IIDs calculated from simulations with varying values of L_{BF}. **C**
929 The number of DCOs observed for different IIDs from simulations involving class I and class
930 II crossovers (CI & CII), class I crossovers only (CI) or class II crossovers only (CII). **D** The
931 proportions of DCOs formed between two class I crossovers (CI_CI), two class II crossovers
932 (CII_CII), or a class I and a class II CO (CI_CII) for different IIDs.
933

Figure 5. Influence of DSB number on crossover patterning and homoeostasis is dependent on the probability of class II crossovers. A-C show results for simulations of wild type meiosis, **D-F** show results for simulation of meiosis with increased class II crossover formation (T2Prob). **A**) Increased DSBs in wild type resulted in more proximal and distal crossovers, but fewer interstitial crossovers. **D**) In mutants with increased class II crossovers, more DSBs resulted in a uniform increase in crossovers. **B-C**) For wild type , CoC values increased at small inter-interval distances with increased DSBs. **E-F**) With increased class II COs, CoC values were ~1 for all inter-interval distances and all DSB numbers. **(G)** Total crossover number for genome-wide simulations using best-fit parameters for male and female meiosis and varying numbers of DSBs. In wild type (dashed lines) increasing DSBs had a minimal effect on total crossovers. With increased class II COs (solid lines) doubling DSBs resulted in twice as many crossovers. Grey shading in CoC curves indicates 95% confidence interval.

Figure 6. Crossover increases tend to accumulate in terminal and proximal regions. A) Terminal regions (e.g. interval 1) experience weaker stress relief than interstitial regions (e.g. interval 8) as they are surrounded by fewer crossovers. Similarly, proximal regions (e.g. interval 5) experience less stress relief, due to the lower precursor number and therefore fewer COs in centromeric regions (interval 4). **B)** As crossovers increase, the additional crossovers tend to accumulate in terminal and proximal regions due to their lower average levels of stress relief.

Table 1. L_{CoC} values

	Mb			µm SC		
	male	female	p value[#]	male	female	p value[#]
experimental	7.05 ± 0.50	12.84 ± 1.50	7.90E-07	11.65 ± 0.86	12.83 ± 1.50	1
simulated	6.30 ± 1.05	11.60 ± 0.83	1.40E-05	10.21 ± 1.75	11.20 ± 0.78	1
p value[#]	1	1		1	1	

[#] Bonferroni multiple-comparison corrected

SUPPLEMENTARY TABLES AND FIGURES

Table S1. Chromosome metrics and beam-film parameters

				Beam-film parameters														
Chr	**Sex**	**Mb**	**µm SC**	**N#**	**B#**	**E#**	**Bs#**	**Be#**	**Bd#**	**Smax^**	**Bsmax#**	**A#**	**L_p^**	**L_{Mb}***	**L_{SC}***	**cL^**	**cR^**	**M#**	**T2prob^**
1	**M**	30.4	49.2	64	1	0.6	0.475	0.5	0.01	8.5	1	1	0.65	19.8	32.0	0.8	1	1	0.005
2	**M**	19.7	31.9	41	1	0.6	0.175	0.225	0.01	7.5	1	1	0.85	16.7	27.1	0.3	0.9	1	0.0065
3	**M**	23.5	37.9	49	1	0.6	0.5	0.65	0.01	5.5	1	1	0.7	16.4	26.6	0.4	0.9	1	0.008
4	**M**	18.6	30.1	39	1	0.6	0.125	0.225	0.01	4	1	1	0.6	11.2	18.0	0.6	0.9	1	0.0055
5	**M**	27.0	43.6	56	1	0.6	0.4	0.5	0.01	9.5	1	1	0.8	21.6	34.9	1.1	0.9	1	0.0065
1	**F**	30.4	25.0	64	1	0.6	0.475	0.5	0.01	8	1	1	1	30.4	25.0	0.7	0.5	1	0.003
2	**F**	19.7	16.2	41	1	0.6	0.175	0.25	0.01	7	1	1	1.6	31.5	25.9	1.2	0.8	1	0.004
3	**F**	23.5	19.3	49	1	0.6	0.5	0.65	0.01	6	1	1	1	23.5	19.3	0.5	0.6	1	0.005
4	**F**	18.6	15.3	39	1	0.6	0.125	0.225	0.01	7	1	1	1.7	31.6	26.0	0.8	0.5	1	0.003
5	**F**	27.0	22.2	56	1	0.6	0.4	0.5	0.01	6.5	1	1	1	27.0	22.2	0.7	0.6	1	0.003
1	**F_{DSB}**	30.4	25.0	38	1	0.6	0.475	0.525	0.01	7	1	1	0.9	27.4	22.5	0.5	0.7	1	0.006
2	**F_{DSB}**	19.7	16.2	38	1	0.6	0.475	0.525	0.01	6.5	1	1	1.5	29.6	24.3	1	0.8	1	0.004
3	**F_{DSB}**	23.5	19.3	29	1	0.6	0.5	0.65	0.01	6	1	1	1	23.5	19.3	0.5	0.6	1	0.008
4	**F_{DSB}**	18.6	15.3	23	1	0.6	0.125	0.225	0.01	6	1	1	1.7	31.6	26.0	0.8	0.4	1	0.005
5	**F_{DSB}**	27.0	22.2	34	1	0.6	0.4	0.5	0.01	8.5	1	1	1.1	29.7	24.4	0.6	0.5	1	0.005

Optimised parameter

^ Fixed parameter

* Calculated based on L_p

964 **Table S2. Beam-film parameters used for simulations shown in each figure.**

			Beam-film parameters												
Figure	**Part**	**Details**	**N**	**B**	**E**	**Bs**	**Be**	**Bd**	**Smax**	**Bsmax**	**A**	**L**	**cL**	**cR**	**M**	**T2prob**
1	**A-D**	male	56	1	0.6	0.4	0.5	0.01	9.5	1	1	0.8	1.1	0.9	1	0.0065
1	**A-D**	female	56	1	0.6	0.4	0.5	0.01	6.5	1	1	1	0.7	0.6	1	0.003
3	**A-C**	L - 0.4	60	1	0.6	0.45	0.55	0.01	7	1	1	0.4	0.8	0.8	1	0.004
3	**A-C**	L - 0.7	60	1	0.6	0.45	0.55	0.01	7	1	1	0.7	0.8	0.8	1	0.004
3	**A-C**	L - 1	60	1	0.6	0.45	0.55	0.01	7	1	1	1	0.8	0.8	1	0.004
3	**A-C**	L - 1.3	60	1	0.6	0.45	0.55	0.01	7	1	1	1.3	0.8	0.8	1	0.004
3	**D-F**	Smax - 3	60	1	0.6	0.45	0.55	0.01	3	1	1	0.7	0.8	0.8	1	0.004
3	**D-F**	Smax - 5	60	1	0.6	0.45	0.55	0.01	5	1	1	0.7	0.8	0.8	1	0.004
3	**D-F**	Smax - 7	60	1	0.6	0.45	0.55	0.01	7	1	1	0.7	0.8	0.8	1	0.004
3	**D-F**	Smax - 9	60	1	0.6	0.45	0.55	0.01	9	1	1	0.7	0.8	0.8	1	0.004
3	**G-I**	T2prob - 0	60	1	0.6	0.45	0.55	0.01	9	1	1	0.7	0.8	0.8	1	0
3	**G-I**	T2prob - 0.002	60	1	0.6	0.45	0.55	0.01	9	1	1	0.7	0.8	0.8	1	0.002
3	**G-I**	T2prob - 0.004	60	1	0.6	0.45	0.55	0.01	9	1	1	0.7	0.8	0.8	1	0.004
3	**G-I**	T2prob - 0.006	60	1	0.6	0.45	0.55	0.01	9	1	1	0.7	0.8	0.8	1	0.006
4	**A-B**	L - 0.8	60	1	0.6	0.45	0.55	0.01	7	1	1	0.8	0.8	0.8	1	0.004
4	**A-B**	L - 0.9	60	1	0.6	0.45	0.55	0.01	7	1	1	0.9	0.8	0.8	1	0.004
4	**A-B**	L - 1	60	1	0.6	0.45	0.55	0.01	7	1	1	1	0.8	0.8	1	0.004
4	**A-B**	L - 1.1	60	1	0.6	0.45	0.55	0.01	7	1	1	1.1	0.8	0.8	1	0.004
4	**C-D**	CI	60	1	0.6	0.45	0.55	0.01	7	1	1	0.7	0.8	0.8	1	0
4	**C-D**	CII	60	1	0.6	0.45	0.55	0.01	0	1	1	0.7	0.8	0.8	1	0.004
4	**C-D**	CI & CII	60	1	0.6	0.45	0.55	0.01	7	1	1	0.7	0.8	0.8	1	0.004
5	**A-C**	wt	30	1	0.6	0.45	0.55	0.01	9	1	1	0.7	0.8	0.8	1	0.004
5	**A-C**	wt	60	1	0.6	0.45	0.55	0.01	9	1	1	0.7	0.8	0.8	1	0.004
5	**A-C**	wt	90	1	0.6	0.45	0.55	0.01	9	1	1	0.7	0.8	0.8	1	0.004
5	**A-C**	wt	120	1	0.6	0.45	0.55	0.01	9	1	1	0.7	0.8	0.8	1	0.004
5	**D-F**	mut	30	1	0.6	0.45	0.55	0.01	9	1	1	0.7	0.8	0.8	1	0.2
5	**D-F**	mut	60	1	0.6	0.45	0.55	0.01	9	1	1	0.7	0.8	0.8	1	0.2
5	**D-F**	mut	90	1	0.6	0.45	0.55	0.01	9	1	1	0.7	0.8	0.8	1	0.2
5	**D-F**	mut	120	1	0.6	0.45	0.55	0.01	9	1	1	0.7	0.8	0.8	1	0.2
5	**G**	wt male - chr 1 - 125 DSBs	32	1	0.6	0.48	0.5	0.01	8.5	1	1	0.65	0.8	1	1	0.005
5	**G**	wt male - chr 2 - 125 DSBs	21	1	0.6	0.18	0.23	0.01	7.5	1	1	0.85	0.3	0.9	1	0.0065
5	**G**	wt male - chr 3 - 125 DSBs	25	1	0.6	0.5	0.65	0.01	5.5	1	1	0.7	0.4	0.9	1	0.008
5	**G**	wt male - chr 4 - 125 DSBs	19	1	0.6	0.13	0.23	0.01	4	1	1	0.6	0.6	0.9	1	0.0055
5	**G**	wt male - chr 5 - 125 DSBs	28	1	0.6	0.4	0.5	0.01	9.5	1	1	0.8	1.1	0.9	1	0.0065
5	**G**	wt male - chr 1 - 250 DSBs	64	1	0.6	0.48	0.5	0.01	8.5	1	1	0.65	0.8	1	1	0.005
5	**G**	wt male - chr 2 - 250 DSBs	42	1	0.6	0.18	0.23	0.01	7.5	1	1	0.85	0.3	0.9	1	0.0065
5	**G**	wt male - chr 3 - 250 DSBs	49	1	0.6	0.5	0.65	0.01	5.5	1	1	0.7	0.4	0.9	1	0.008
5	**G**	wt male - chr 4 - 250 DSBs	39	1	0.6	0.13	0.23	0.01	4	1	1	0.6	0.6	0.9	1	0.0055
5	**G**	wt male - chr 5 - 250 DSBs	56	1	0.6	0.4	0.5	0.01	9.5	1	1	0.8	1.1	0.9	1	0.0065
5	**G**	wt male - chr 1 - 375 DSBs	96	1	0.6	0.48	0.5	0.01	8.5	1	1	0.65	0.8	1	1	0.005
5	**G**	wt male - chr 2 - 375 DSBs	63	1	0.6	0.18	0.23	0.01	7.5	1	1	0.85	0.3	0.9	1	0.0065
5	**G**	wt male - chr 3 - 375 DSBs	75	1	0.6	0.5	0.65	0.01	5.5	1	1	0.7	0.4	0.9	1	0.008
5	**G**	wt male - chr 4 - 375 DSBs	57	1	0.6	0.13	0.23	0.01	4	1	1	0.6	0.6	0.9	1	0.0055
5	**G**	wt male - chr 5 - 375 DSBs	84	1	0.6	0.4	0.5	0.01	9.5	1	1	0.8	1.1	0.9	1	0.0065
5	**G**	wt male - chr 1 - 500 DSBs	128	1	0.6	0.48	0.5	0.01	8.5	1	1	0.65	0.8	1	1	0.005
5	**G**	wt male - chr 2 - 500 DSBs	84	1	0.6	0.18	0.23	0.01	7.5	1	1	0.85	0.3	0.9	1	0.0065
5	**G**	wt male - chr 3 - 500 DSBs	98	1	0.6	0.5	0.65	0.01	5.5	1	1	0.7	0.4	0.9	1	0.008
5	**G**	wt male - chr 4 - 500 DSBs	78	1	0.6	0.13	0.23	0.01	4	1	1	0.6	0.6	0.9	1	0.0055
5	**G**	wt male - chr 5 - 500 DSBs	112	1	0.6	0.4	0.5	0.01	9.5	1	1	0.8	1.1	0.9	1	0.0065
5	**G**	mut male - chr 1 - 125 DSBs	32	1	0.6	0.48	0.5	0.01	8.5	1	1	0.65	0.8	1	1	0.2

5	**G**	mut male - chr 2 - 125 DSBs	21	1	0.6	0.18	0.23	0.01	7.5	1	1	0.85	0.3	0.9	1	0.2
5	**G**	mut male - chr 3 - 125 DSBs	25	1	0.6	0.5	0.65	0.01	5.5	1	1	0.7	0.4	0.9	1	0.2
5	**G**	mut male - chr 4 - 125 DSBs	19	1	0.6	0.13	0.23	0.01	4	1	1	0.6	0.6	0.9	1	0.2
5	**G**	mut male - chr 5 - 125 DSBs	28	1	0.6	0.4	0.5	0.01	9.5	1	1	0.8	1.1	0.9	1	0.2
5	**G**	mut male - chr 1 - 250 DSBs	64	1	0.6	0.48	0.5	0.01	8.5	1	1	0.65	0.8	1	1	0.2
5	**G**	mut male - chr 2 - 250 DSBs	42	1	0.6	0.18	0.23	0.01	7.5	1	1	0.85	0.3	0.9	1	0.2
5	**G**	mut male - chr 3 - 250 DSBs	49	1	0.6	0.5	0.65	0.01	5.5	1	1	0.7	0.4	0.9	1	0.2
5	**G**	mut male - chr 4 - 250 DSBs	39	1	0.6	0.13	0.23	0.01	4	1	1	0.6	0.6	0.9	1	0.2
5	**G**	mut male - chr 5 - 250 DSBs	56	1	0.6	0.4	0.5	0.01	9.5	1	1	0.8	1.1	0.9	1	0.2
5	**G**	mut male - chr 1 - 375 DSBs	96	1	0.6	0.48	0.5	0.01	8.5	1	1	0.65	0.8	1	1	0.2
5	**G**	mut male - chr 2 - 375 DSBs	63	1	0.6	0.18	0.23	0.01	7.5	1	1	0.85	0.3	0.9	1	0.2
5	**G**	mut male - chr 3 - 375 DSBs	75	1	0.6	0.5	0.65	0.01	5.5	1	1	0.7	0.4	0.9	1	0.2
5	**G**	mut male - chr 4 - 375 DSBs	57	1	0.6	0.13	0.23	0.01	4	1	1	0.6	0.6	0.9	1	0.2
5	**G**	mut male - chr 5 - 375 DSBs	84	1	0.6	0.4	0.5	0.01	9.5	1	1	0.8	1.1	0.9	1	0.2
5	**G**	mut male - chr 1 - 500 DSBs	128	1	0.6	0.48	0.5	0.01	8.5	1	1	0.65	0.8	1	1	0.2
5	**G**	mut male - chr 2 - 500 DSBs	84	1	0.6	0.18	0.23	0.01	7.5	1	1	0.85	0.3	0.9	1	0.2
5	**G**	mut male - chr 3 - 500 DSBs	98	1	0.6	0.5	0.65	0.01	5.5	1	1	0.7	0.4	0.9	1	0.2
5	**G**	mut male - chr 4 - 500 DSBs	78	1	0.6	0.13	0.23	0.01	4	1	1	0.6	0.6	0.9	1	0.2
5	**G**	mut male - chr 5 - 500 DSBs	112	1	0.6	0.4	0.5	0.01	9.5	1	1	0.8	1.1	0.9	1	0.2
5	**G**	wt female - chr 1 - 125 DSBs	32	1	0.6	0.48	0.5	0.01	8	1	1	1	0.7	0.5	1	0.003
5	**G**	wt female - chr 2 - 125 DSBs	21	1	0.6	0.18	0.25	0.01	7	1	1	1.6	1.2	0.8	1	0.004
5	**G**	wt female - chr 3 - 125 DSBs	25	1	0.6	0.5	0.65	0.01	6	1	1	1	0.5	0.6	1	0.005
5	**G**	wt female - chr 4 - 125 DSBs	19	1	0.6	0.13	0.23	0.01	7	1	1	1.7	0.8	0.5	1	0.003
5	**G**	wt female - chr 5 - 125 DSBs	28	1	0.6	0.4	0.5	0.01	6.5	1	1	1	0.7	0.6	1	0.003
5	**G**	wt female - chr 1 - 250 DSBs	64	1	0.6	0.48	0.5	0.01	8	1	1	1	0.7	0.5	1	0.003
5	**G**	wt female - chr 2 - 250 DSBs	42	1	0.6	0.18	0.25	0.01	7	1	1	1.6	1.2	0.8	1	0.004
5	**G**	wt female - chr 3 - 250 DSBs	49	1	0.6	0.5	0.65	0.01	6	1	1	1	0.5	0.6	1	0.005
5	**G**	wt female - chr 4 - 250 DSBs	39	1	0.6	0.13	0.23	0.01	7	1	1	1.7	0.8	0.5	1	0.003
5	**G**	wt female - chr 5 - 250 DSBs	56	1	0.6	0.4	0.5	0.01	6.5	1	1	1	0.7	0.6	1	0.003
5	**G**	wt female - chr 1 - 375 DSBs	96	1	0.6	0.48	0.5	0.01	8	1	1	1	0.7	0.5	1	0.003
5	**G**	wt female - chr 2 - 375 DSBs	63	1	0.6	0.18	0.25	0.01	7	1	1	1.6	1.2	0.8	1	0.004
5	**G**	wt female - chr 3 - 375 DSBs	75	1	0.6	0.5	0.65	0.01	6	1	1	1	0.5	0.6	1	0.005
5	**G**	wt female - chr 4 - 375 DSBs	57	1	0.6	0.13	0.23	0.01	7	1	1	1.7	0.8	0.5	1	0.003
5	**G**	wt female - chr 5 - 375 DSBs	84	1	0.6	0.4	0.5	0.01	6.5	1	1	1	0.7	0.6	1	0.003
5	**G**	wt female - chr 1 - 500 DSBs	128	1	0.6	0.48	0.5	0.01	8	1	1	1	0.7	0.5	1	0.003
5	**G**	wt female - chr 2 - 500 DSBs	84	1	0.6	0.18	0.25	0.01	7	1	1	1.6	1.2	0.8	1	0.004
5	**G**	wt female - chr 3 - 500 DSBs	98	1	0.6	0.5	0.65	0.01	6	1	1	1	0.5	0.6	1	0.005
5	**G**	wt female - chr 4 - 500 DSBs	78	1	0.6	0.13	0.23	0.01	7	1	1	1.7	0.8	0.5	1	0.003
5	**G**	wt female - chr 5 - 500 DSBs	112	1	0.6	0.4	0.5	0.01	6.5	1	1	1	0.7	0.6	1	0.003
5	**G**	mut female - chr 1 - 125 DSBs	32	1	0.6	0.48	0.5	0.01	8	1	1	1	0.7	0.5	1	0.2
5	**G**	mut female - chr 2 - 125 DSBs	21	1	0.6	0.18	0.25	0.01	7	1	1	1.6	1.2	0.8	1	0.2
5	**G**	mut female - chr 3 - 125 DSBs	25	1	0.6	0.5	0.65	0.01	6	1	1	1	0.5	0.6	1	0.2

5	**G**	mut female - chr 4 - 125 DSBs	19	1	0.6	0.13	0.23	0.01	7	1	1	1.7	0.8	0.5	1	0.2
5	**G**	mut female - chr 5 - 125 DSBs	28	1	0.6	0.4	0.5	0.01	6.5	1	1	1	0.7	0.6	1	0.2
5	**G**	mut female - chr 1 - 250 DSBs	64	1	0.6	0.48	0.5	0.01	8	1	1	1	0.7	0.5	1	0.2
5	**G**	mut female - chr 2 - 250 DSBs	42	1	0.6	0.18	0.25	0.01	7	1	1	1.6	1.2	0.8	1	0.2
5	**G**	mut female - chr 3 - 250 DSBs	49	1	0.6	0.5	0.65	0.01	6	1	1	1	0.5	0.6	1	0.2
5	**G**	mut female - chr 4 - 250 DSBs	39	1	0.6	0.13	0.23	0.01	7	1	1	1.7	0.8	0.5	1	0.2
5	**G**	mut female - chr 5 - 250 DSBs	56	1	0.6	0.4	0.5	0.01	6.5	1	1	1	0.7	0.6	1	0.2
5	**G**	mut female - chr 1 - 375 DSBs	96	1	0.6	0.48	0.5	0.01	8	1	1	1	0.7	0.5	1	0.2
5	**G**	mut female - chr 2 - 375 DSBs	63	1	0.6	0.18	0.25	0.01	7	1	1	1.6	1.2	0.8	1	0.2
5	**G**	mut female - chr 3 - 375 DSBs	75	1	0.6	0.5	0.65	0.01	6	1	1	1	0.5	0.6	1	0.2
5	**G**	mut female - chr 4 - 375 DSBs	57	1	0.6	0.13	0.23	0.01	7	1	1	1.7	0.8	0.5	1	0.2
5	**G**	mut female - chr 5 - 375 DSBs	84	1	0.6	0.4	0.5	0.01	6.5	1	1	1	0.7	0.6	1	0.2
5	**G**	mut female - chr 1 - 500 DSBs	128	1	0.6	0.48	0.5	0.01	8	1	1	1	0.7	0.5	1	0.2
5	**G**	mut female - chr 2 - 500 DSBs	84	1	0.6	0.18	0.25	0.01	7	1	1	1.6	1.2	0.8	1	0.2
5	**G**	mut female - chr 3 - 500 DSBs	98	1	0.6	0.5	0.65	0.01	6	1	1	1	0.5	0.6	1	0.2
5	**G**	mut female - chr 4 - 500 DSBs	78	1	0.6	0.13	0.23	0.01	7	1	1	1.7	0.8	0.5	1	0.2
5	**G**	mut female - chr 5 - 500 DSBs	112	1	0.6	0.4	0.5	0.01	6.5	1	1	1	0.7	0.6	1	0.2
S1 & S2	**chr1**	male	64	1	0.6	0.48	0.5	0.01	8.5	1	1	0.65	0.8	1	1	0.005
S1 & S2	**chr1**	female	64	1	0.6	0.48	0.5	0.01	8	1	1	1	0.7	0.5	1	0.003
S1 & S2	**chr2**	male	41	1	0.6	0.18	0.23	0.01	7.5	1	1	0.85	0.3	0.9	1	0.0065
S1 & S2	**chr2**	female	41	1	0.6	0.18	0.25	0.01	7	1	1	1.6	1.2	0.8	1	0.004
S1 & S2	**chr3**	male	49	1	0.6	0.5	0.65	0.01	5.5	1	1	0.7	0.4	0.9	1	0.008
S1 & S2	**chr3**	female	49	1	0.6	0.5	0.65	0.01	6	1	1	1	0.5	0.6	1	0.005
S1 & S2	**chr4**	male	39	1	0.6	0.13	0.23	0.01	4	1	1	0.6	0.6	0.9	1	0.0055
S1 & S2	**chr4**	female	39	1	0.6	0.13	0.23	0.01	7	1	1	1.7	0.8	0.5	1	0.003
S1 & S2	**chr5**	male	56	1	0.6	0.4	0.5	0.01	9.5	1	1	0.8	1.1	0.9	1	0.0065
S1 & S2	**chr5**	female	56	1	0.6	0.4	0.5	0.01	6.5	1	1	1	0.7	0.6	1	0.003
S3	**chr5**	low	56	1	0.6	0.4	0.5	0.01	3	1	1	1.7	0.1	0.1	1	0.002
S3	**chr5**	high	56	1	0.6	0.4	0.5	0.01	10	1	1	0.4	1.3	1.3	1	0.006
S4		CI - all	60	1	0.6	0.45	0.55	0.01	7	1	1	0.7	0.8	0.8	1	0
S4		CII - T2Prob 0.001	60	1	0.6	0.45	0.55	0.01	0	1	1	0.7	0.8	0.8	1	0.001
S4		CI & CII - T2Prob 0.001	60	1	0.6	0.45	0.55	0.01	7	1	1	0.7	0.8	0.8	1	0.001
S4		CII - T2Prob 0.005	60	1	0.6	0.45	0.55	0.01	0	1	1	0.7	0.8	0.8	1	0.005
S4		CI & CII - T2Prob 0.005	60	1	0.6	0.45	0.55	0.01	7	1	1	0.7	0.8	0.8	1	0.005
S4		CII - T2Prob 0.01	60	1	0.6	0.45	0.55	0.01	0	1	1	0.7	0.8	0.8	1	0.01
S4		CI & CII - T2Prob 0.01	60	1	0.6	0.45	0.55	0.01	7	1	1	0.7	0.8	0.8	1	0.01
S4		CII - T2Prob 0.025	60	1	0.6	0.45	0.55	0.01	0	1	1	0.7	0.8	0.8	1	0.025
S4		CI & CII - T2Prob 0.025	60	1	0.6	0.45	0.55	0.01	7	1	1	0.7	0.8	0.8	1	0.025

S4	CII - T2Prob 0.125	60	1	0.6	0.45	0.55	0.01	0	1	1	0.7	0.8	0.8	1	0.125
S4	CI & CII - T2Prob 0.125	60	1	0.6	0.45	0.55	0.01	7	1	1	0.7	0.8	0.8	1	0.125

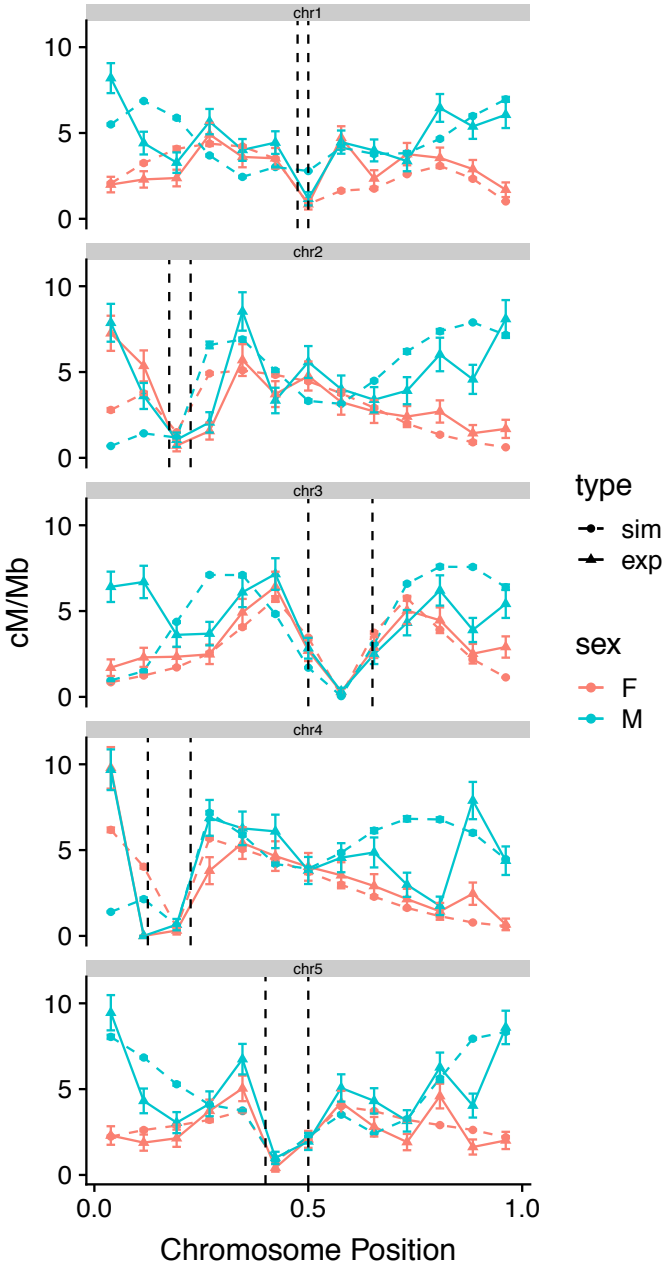

966

967

968 **Figure S1. Experimental and simulated crossover distributions.** Each analysis includes
969 experimental (solid lines) and simulated (dashed lines) data for male (blue) and female (orange). Dashed
970 lines represent the limits of the centromeric region over which precursor (DSB) number is markedly
971 reduced both biologically (38) and during simulations. Male and female simulations shown, assume
972 250 DSBs genome-wide. Chromosomes were divided into 13 equal-sized adjacent intervals for
973 analysis.

974

975

976

977 **Figure S2. CoC curves for simulated and experimental recombination data.** Each analysis

978 includes experimental (solid lines) and simulated (dashed lines) data for male (blue) and female

979 (orange). CoC curves with inter-interval distance measured in either Mb or μm SC are shown. Male

980 curves are shifted to the right relative to female curves when inter-interval distance is measured in

981 Mb, but are similar when inter-interval distance is measured in μm SC. Male and female simulations

982 shown assume 250 DSBs genome-wide. Chromosomes were divided into 13 equal-sized adjacent

983 intervals for analysis

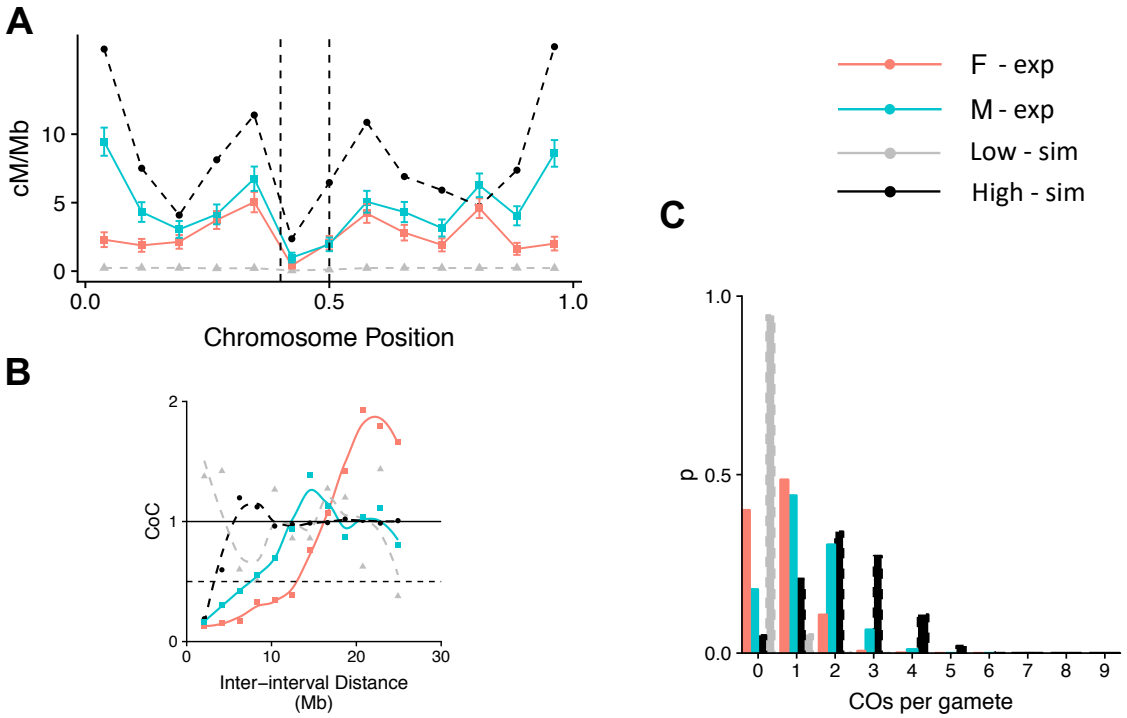

Figure S3. Examples of simulated data that did not fit experimental data. Each analysis shows experimental (solid lines) for male (blue) and female (orange) and simulated (dashed lines) data for high (black) and low (grey) recombining parameter sets. **A** Crossover distributions for Arabidopsis chromosome 5. Dashed lines represent the limits of the centromeric region over which precursor (DSB) number is markedly reduced both biologically (38) and during simulations. Error bars indicate 95% confidence intervals. **B** CoC curves for chromosome 5 with inter-interval distance (IID, the distance between a pair of genetic intervals) measured in Mb. **C** Event distribution for chromosome 5. Simulations shown assume 250 DSBs genome-wide. Chromosomes were divided into 13 equal-sized adjacent intervals for analysis.

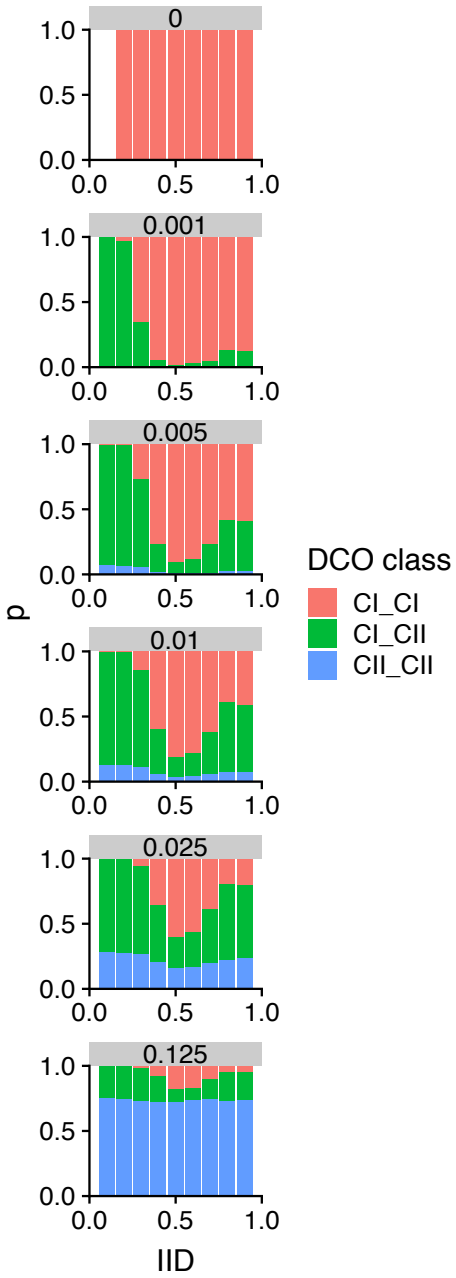

996

997 **Figure S4. Proportions of different double crossover (DCO) classes.** Charts show the proportions of
998 DCOs formed between two class I crossovers (CI_CI), two class II crossovers (CII_CII), or a class I and a
999 class II CO (CI_CII) for different IIDs and different values of T2Prob (grey bars). Total proportion of class
1000 II crossovers are as follows: T2Prob = 0, 0% class II COs; T2Prob = 0.001, 3% class II COs; T2Prob =
1001 0.005, 13% class II COs; T2Prob = 0.01, 23% class II COs; T2Prob = 0.025, 43% class II COs; T2Prob =
1002 0.125, 81% class II COs.